Marine and Petroleum Geology 173 (2025) 107292

Contents lists available at ScienceDirect

Marine and Petroleum Geology

journal homepage: www.elsevier.com/locate/marpetgeo

The tectonic evolution of the pre-Mesozoic key period in the Tarim Basin: Constraints from U-Pb geochronology of paleozoic detrital zircons in the central uplift zone

Yang Gao [a,b,c,d], Lin Jiang [a,c,d,*], Weiyan Chen [c,d], Hongkui Dong [c], Wen Zhao [c], Fujie Jiang [a,b], Qingong Zhuo [c,d], Haizu Zhang [e], Yao Hu [a,b,c,d], Zhou Fang [a,b], Xiaohao Wang [a,b], Yingqi Feng [c,d]

[a] State Key Laboratory of Petroleum Resources and Engineering, China University of Petroleum (Beijing), Beijing, 102249, China
[b] College of Geosciences, China University of Petroleum (Beijing), Beijing, 102249, China
[c] PetroChina Research Institute of Petroleum Exploration and Development, Beijing, 10083, China
[d] CNPC Key Laboratory of Basin Structure and Hydrocarbon Accumulation, Beijing, 10083, China
[e] PetroChina Tarim Oilfield Company, Korla, 841000, China

ARTICLE INFO

Keywords:
Tarim craton
Detrital zircon
Mountain building
Provenance
U-Pb chronology

ABSTRACT

In recent years, as oil and gas exploration has increasingly advanced into deeper layers, the tectonic evolution of the Tarim Basin before the Mesozoic has garnered significant attention. However, due to the scarcity of magmatic and metamorphic records within the basin, analyses of major tectonic events remain contentious. Orogenic events contribute substantial detrital material to nearby regions, which is consequently reflected in the detrital zircon record. This study focuses on the sedimentary strata of the central uplift zone of the Tarim Basin. U-Pb dating was conducted on 600 detrital zircon grains from the Silurian to the Carboniferous periods, revealing two main age peaks at 806Ma and 452Ma. No significant peaks were observed in the age distribution outside of these two regions. The Paleozoic zircon data obtained from this study, when combined with previously published U-Pb age data of 2155 detrital zircons from southern and northern Tarim, indicate that these ages do not correlate with the Grenville orogeny event occurring between 1300Ma and 900Ma. Thus, the impact of the Grenville orogeny on the Tarim Craton appears to be very limited. The peak around 800 Ma generated by all zircon data corresponds to the transition period from the breakup of the Rodinia supercontinent to the formation of Gondwana. The collisional assembly of the north and south Tarim terranes likely occurred between 900 and 820Ma, during which the collisional orogeny led to the formation of the central uplift zone in Tarim. In the Paleozoic, the sediment sources of the central uplift zone in Tarim primarily originated within Tarim itself, with additional influences from the West Kunlun orogenic belt, South Tianshan, and Altun orogenic belt.

1. Introduction

Tarim Basin, located in northwest China, is a large superimposed basin with Precambrian metamorphic basement and Neoproterozoic to Cenozoic sedimentary cover (Jia, 2009; Long et al., 2010; He et al., 2014). In recent years, as hydrocarbon exploration has progressively advanced to deeper formations, three primary source rock intervals have been identified in the Tarim Basin: the Lower Cambrian, Carboniferous-Permian, and Triassic-Jurassic. Additionally, hydrocarbon shows have been successively discovered in Paleozoic intervals such as the Cambrian, Ordovician, and Silurian formations. However, due to the impact of multiple tectonic events, the pre-Mesozoic structural configuration of the Tarim Basin and its influencing factors remain unclear. Core issues such as the Paleozoic tectonic evolution of Tarim and the nature of the Precambrian basement of the Tarim Basin are still under debate, hindering the progress of petroleum exploration.

The evolution of the Precambrian basement in the Tarim Basin is primarily associated with two critical periods: the Rodinia and Columbia supercontinents. However, due to a lack of reliable paleomagnetic data, paleontological evidence, and magmatic-metamorphic records within

* Corresponding author. State Key Laboratory of Petroleum Resources and Engineering, China University of Petroleum (Beijing), Beijing, 102249, China.
E-mail address: jianglin01@petrochina.com.cn (L. Jiang).

https://doi.org/10.1016/j.marpetgeo.2025.107292
Received 11 August 2024; Received in revised form 23 December 2024; Accepted 7 January 2025
Available online 15 January 2025

the basin, current reconstructions of the tectonic framework during these periods largely rely on analysis and testing of magmatic rock outcrops found in the field. This approach allows scholars to infer plate affinities, ocean-continent transition phases, and processes of supercontinental breakup and amalgamation, thereby enabling a more detailed reconstruction of the Tarim Craton's evolution (Zhang et al., 2009; Xu et al., 2013; Ge et al., 2014; Zhao et al., 2021; Wu et al., 2022). Due to the limited number of such magmatic rock outcrops and the interpretive ambiguity among scholars regarding experimental results, the tectonic framework of these two critical periods remains contentious: (1) A consensus has been reached that the Tarim Craton comprises a collage of the north and south Tarim terranes; however, the exact timing of their assembly-whether during the Rodinia or Columbia supercontinent periods-remains debated; (2) If the amalgamation occurred during the Rodinia period, an additional question arises regarding the nature of the relationship between the Tarim Craton and the Rodinia supercontinent. Some scholars suggest that the collisional assembly of the north and south Tarim terranes occurred around 800 Ma, corresponding to the timing of the Rodinia supercontinent breakup (Guo et al., 2005; Zhang et al., 2009; Zhao et al., 2021). At the same time, some scholars also argue that the south and north Tarim terranes had already completed their amalgamation by around 1800 Ma, corresponding to the formation of the Columbia supercontinent (Yang et al., 2014; Li et al., 2019; Wu et al., 2020).

Another key tectonic period in the Tarim Basin prior to the Mesozoic is the Paleozoic, which corresponds to the primary target intervals in current deep to ultra-deep exploration efforts. The Tarim Basin has experienced the opening, subduction and collision orogeny of the Paleo-Asian Ocean and the Tethys Ocean since the Neoproterozoic (Jia and Wei, 2002; Shu et al., 2011; Xu et al., 2011). It can be seen that the coupling relationship between the Tarim Craton and the peripheral orogenic belt is very complex, which is controlled by the superposition and transformation of different tectonic evolution in multiple periods. The Paleozoic tectonic framework of the Tarim Basin has long been debated, primarily due to the presence of three dynamic sources during this period: first, the subduction and consumption of the Proto-Tethys Ocean along the southern margin of the basin (Zhang et al., 2019; Gao et al., 2024); second, the subduction and consumption of the South Tianshan Ocean along the northern margin (Carroll et al., 2001; Wang et al., 2011; Ge et al., 2012a,b; Lin et al., 2013); and third, the subduction and consumption of the Altyn Ocean along the southeastern margin of the basin. Identifying the links between the basin and the tectonic evolution of various orogenic belts is crucial to unraveling the complex Paleozoic basin-mountain relationships in the Tarim Basin.

Detrital zircon, due to its high closure temperature, stable mineral properties, and strong resistance to thermal alteration, is widely distributed in igneous, metamorphic, and sedimentary rocks. It has been extensively used in recent years to study provenance, plate tectonics, and the formation and evolution of orogenic belts, as it can provide crucial information about the characteristics of the parent rock and its depositional age (Eizenhöfer et al., 2014, 2015; Eizenhöfer and Zhao, 2018; Chen et al., 2020; Wang et al., 2020a,b; Feng et al., 2023). Sedimentary strata buried thousands of meters underground record the lithological changes from the basement to the surface, providing more effective constraints for understanding long-term geological evolution. Previous studies have predominantly focused on the typical igneous rocks exposed in the northern and southern Tarim Basin, with relatively little attention given to the sedimentary cover of the central uplift. Compared to igneous rocks, sedimentary rocks are less advantageous in indicating specific large-scale tectonic events. However, for the central Tarim Basin, even if this region received distal sediments at a particular time, records of major tectonic events, such as the collisional assembly of the north and south Tarim terranes, would certainly be preserved within the sedimentary deposits. Therefore, the advantage of selecting Paleozoic detrital zircon samples from within the central uplift zone for this study lies in its location at the junction of the south and north Tarim terranes. This positioning allows it to capture zircons from contemporaneous outcrops of igneous and sedimentary strata in adjacent areas, without the need to rely on the currently typical outcrops of the south and north Tarim terranes for indicators.

Focusing on the Paleozoic sediments in the central uplift of Tarim Basin, this paper presents a detailed chronological analysis of detrital zircon U-Pb dating based on existing literature. There are two directions in this paper. Firstly, by analyzing the peak ages and distribution of detrital zircons, the study further focuses on the pre-Paleozoic major tectonic events in the central Tarim Basin, proposing a model for the collision between the south and north Tarim terranes. Secondly, by analyzing the characteristics of provenance changes during different Paleozoic periods, the study further investigates and clarifies the tectonic evolution history of central Tarim during these periods, proposing the Paleozoic basin-mountain coupling relationships between Tarim and the surrounding orogenic belts.

2. Geological settings

Tarim Basin is one of the three cratons in China. It is surrounded by three orogenic belts: Tianshan Mountain in the north, Altun Mountain in the southeast and Kunlun Mountain in the southwest (Fig. 1. A). The Tarim Basin exhibits a typical double-layered structure, consisting of a Precambrian crystalline basement and a sedimentary cover that has accumulated since the Neoproterozoic (Jia et al., 2009). The Precambrian tectonic evolution of the Tarim Basin can be divided into three stages: the first is the Archean basement evolution stage (Long et al., 2010; Zong et al., 2013; Guo et al., 2013; He et al., 2014); the second is the Mesoproterozoic response stage of the Tarim Basin to the assembly and breakup of the Columbia supercontinent (Shu et al., 2011; Long et al., 2012; Ge et al., 2013; Wang et al., 2020a,b; Wu et al., 2020; Guo et al., 2022, 2023); and the third is the Neoproterozoic response stage to the assembly and breakup of the Rodinia supercontinent (Xu et al., 2013; Wen et al., 2018; He et al., 2019; Zhao et al., 2021; Li et al., 2025). These three stages correspond to multiple magmatic and metamorphic events discovered in the Tarim Basin and its surrounding areas, with key dates primarily including the Late Archean (2.8-2.5Ga), the Middle Paleoproterozoic (2.0-1.8Ga), and the Neoproterozoic (1000-600 Ma).

In recent years, with the continuous advancement of Precambrian geological research in the Tarim Basin, many scholars have obtained ages for late Archean TTG (tonalite-trondhjemite-granodiorite) rocks and granites. For instance, Long et al. (2010) obtained an age of 2516 Ma for TTG rocks and granitic gneisses in the Kuruktag area. Zong et al. (2013) reported TTG rock ages of 2.7–2.6 Ga in the Dunhuang region. At the same time, these TTG rocks exhibit geochemical characteristics similar to those of volcanic island arcs, suggesting that the Tarim region experienced a subduction-related tectonic thermal event during the late Archean.

The mid-Proterozoic (2.0–1.8 Ga) Tarim Basin is considered to have been involved in subduction-accretion and collision processes associated with the Columbia supercontinent (Zhang et al., 2007; Shu et al., 2011; Chen et al., 2013; Ge et al., 2013; He et al., 2014; Yang et al., 2018). However, these data are primarily derived from outcrops in the northeastern or southwestern parts of the Tarim Basin. Ge et al. (2013) proposed the existence of two orogenic belts in the mid-Proterozoic Tarim, including a northern orogenic belt with ages between 1.9 and 1.8 Ga and a southern orogenic belt with ages between 2.0 and 1.9 Ga. Chen et al. (2013) suggested two subduction-collision events in the Proterozoic, occurring at 1.95–1.90 Ga and 1.82–1.80 Ga. Shu et al. (2011) obtained a U-Pb age of 1931Ma for granitic gneiss in the Kuruktag region of Tarim, while He et al. (2014) discovered a significant 1900 Ma peak of metamorphic zircons in Neoproterozoic strata in northwestern Tarim. Additionally, Zhang et al. (2007) reported granites dated to 2.4-2.3Ga in the foreland of the West Kunlun Mountains in southwestern Tarim and found zircon overgrowth ages of 1.9Ga. Yang et al. (2018) obtained an age of approximately 1920 Ma for granites from drill cores in the central

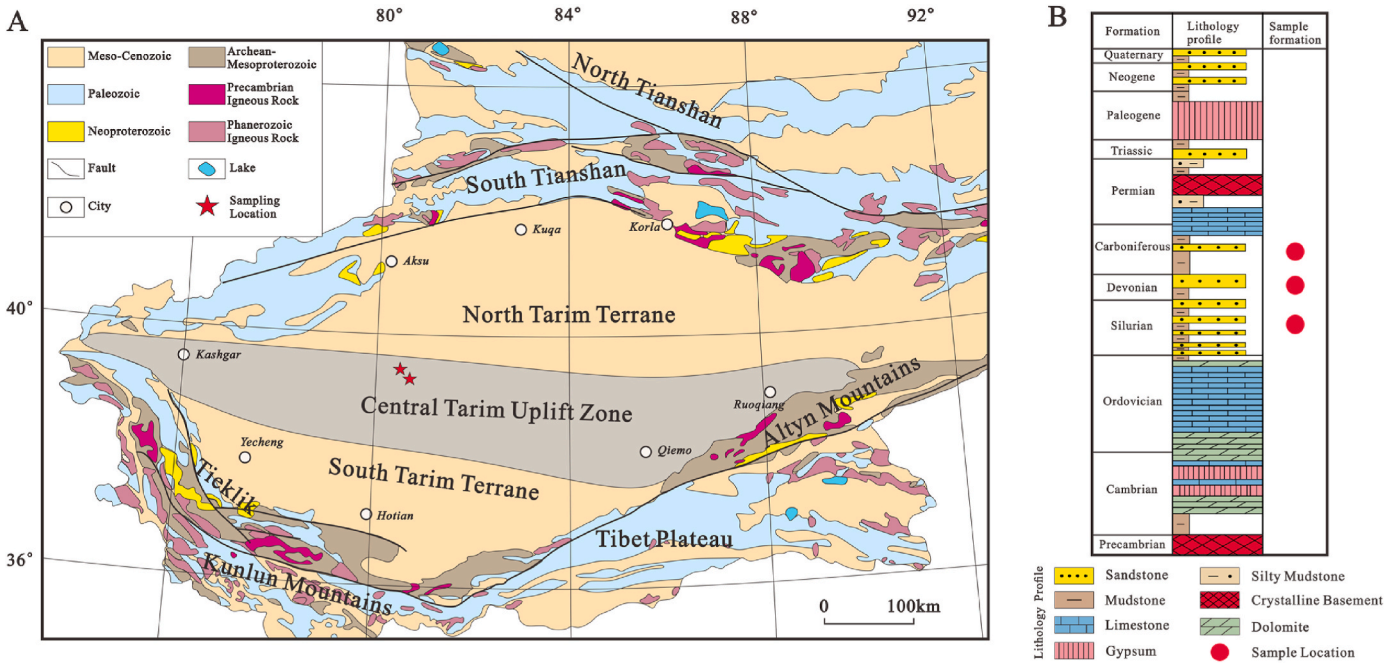

Fig. 1. A. Geological map of Tarim Craton and its surrounding areas (modified after Xu et al., 2013); B. Lithologic column diagram of the central Tarim Basin.

Tarim terrane. These age findings indicate that an important tectono-thermal event occurred in the Tarim during the mid-Proterozoic.

During the Neoproterozoic, the Tarim Basin recorded a significant number of magmatic and metamorphic events associated with the evolution of the Rodinia supercontinent (Ge et al., 2012a,b; Han et al., 2012; Zhao et al., 2021; Wu et al., 2022; Li et al., 2025). Li et al. (2025) discovered granitic ages of approximately 920 Ma along the margins of the Tarim Basin and interpreted them as products of a subduction-related setting. Zhao et al. (2021) used paleomagnetic data to show that there was a latitudinal difference of 28° between South Tarim and North Tarim at 900 Ma, and they constrained the suturing time of the two terranes to between 870 and 820 Ma. Wu et al. (2022) suggested that around 830–790 Ma, subduction of the northern margin of the Tarim Craton beneath the Ili-Central Tian Shan region led to syn-collisional magmatic activity. Xu et al. (2005) found bimodal volcanic rock ages of 755 Ma in the Beiyixi Formation in the northeastern Tarim, interpreting this period as corresponding to a rifting environment in the northeastern part of the Tarim Basin. Ge et al. (2012) obtained granite ages of 660-630 Ma in the Kuruktag region and associated them with the amalgamation of the Gondwana supercontinent.

During the Paleozoic, the Tarim Basin experienced complex tectonic movements, including the subduction and consumption of the oceanic crust of the proto-Tethys Ocean and the South Tianshan Ocean, as well as continent-continent collisions and compression. These tectonic events left extensive magmatic records both in the orogenic belts and within the basin. For instance, Kang et al. (2013) identified granites with a formation age of 450Ma in the South Altyn region. Ge et al. (2012) identified granodiorite in the Korla region with a crystallization age of 420Ma, inferring that the initiation of South Tianshan Ocean subduction occurred before 420Ma. Similarly, Chen et al., 2020 discovered granite dated to approximately 477Ma in central West Kunlun, interpreting it as a product of the Proto-Tethys Ocean subduction.

The central uplift zone is an important tectonic unit in the Tarim Basin, which consists of three secondary tectonic units: Bachu Uplift, Tazhong Uplift and Tadong uplift. The sampling points of this study are located in the Carboniferous to Silurian strata of Bachu Uplift (Fig. 1. B). In the Silurian period, the Bachu area was a shallow-littoral-continental clastic sedimentary environment with light gray sandstone and brown mudstone as the main lithology. In the Devonian period, it is mainly a light gray gravelly sandstone and a fine sandstone. In the Carboniferous period, mudstone, limestone and sandstone were developed, and the sedimentary environment was mainly coastal shallow sea, open platform and continental sedimentary environment.

3. Sampling and methods

We collected six core samples from the Carboniferous to Silurian systems from two wells in the Bachu Uplift, a secondary tectonic unit of the central uplift. It consists of four Silurian sandstones (H3-2855.01, H3-3241.5, H3-3404.5, H3-3410.1), one Devonian sandstone (Ht1-3632.18), and one carboniferous sandstone (Ht1-3423.0) (Fig. 2). The locations of the two wells are indicated on the map (Sampling Location of Fig. 1). The lithologic column of the six samples is shown in Fig. 2. It can be observed that interbedding of sandstone and mudstone layers is frequent in the Silurian and the lowest Carboniferous strata, and a pattern also reflected in thin sections A and B (Fig. 2). This phenomenon may result from intense tectonic activity during these periods, which created unstable depositional environments and led to rapid changes in sedimentary conditions. From the observation of photomicrograph, it is evident that the grain size of H3-2855.01 is significantly smaller than that of H3-3404.5. This difference may be attributed to the distinct provenance of the sediments, suggesting that they originated from different sources. Additionally, the grain size of the Devonian sample Ht1-3632.18 is similar to that of H3-3404.5, with both exhibiting poor roundness, possibly indicating a similar provenance. During sediment transport, larger grains tend to settle more readily, while finer grains can be carried further. Based on this, we infer that the tectonic configuration during the deposition of H3-2855.01 and H3-3404.5 may have changed. Furthermore, the tectonic configuration during the deposition of H3-3404.5 and Ht1-3632.18 appears to be similar, as these two samples likely received sediment sources located closer than those of H3-2855.01.

Each sandstone sample was processed following traditional procedures, starting with mechanical crushing and washing. The samples were then treated using heavy liquid separation and magnetic separation techniques. Approximately 200 zircon grains were manually selected under a microscope and fixed onto double-sided adhesive tape, which was then embedded in epoxy resin to create a mount. After the epoxy

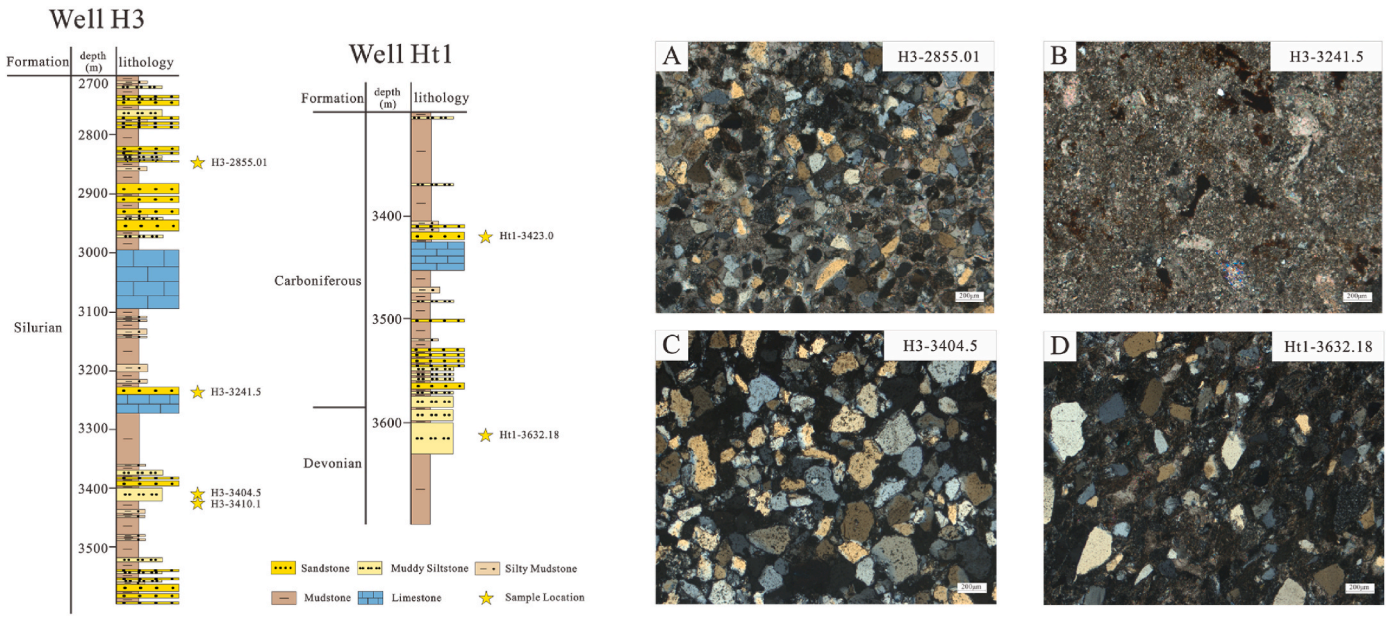

Fig. 2. Core column diagram and sampling location of the well (left), thin section photomicrographs of samples (Right).

resin had fully cured, the mount was polished to reveal the zircon surfaces and internal structures. Subsequently, transmitted, reflected, and cathodoluminescence (CL) images were taken, and zircon grains without cracks or inclusions were selected for further age testing.

Zircon U-Pb dating was completed on the Laser denudation inductively coupled Plasma Mass Spectrometer (LA-ICP-MS) at the Laboratory of Basin Tectonics and Oil and Gas Accumulation, Petroleum Geology Experimental Research Center, Research Institute of Petroleum Exploration and Development, China. NWV 193 nm laser and Element SF-ICP-MS mass spectrometer are used. Based on the transmitted, reflected, and cathodoluminescence (CL) images, the ablation spots were determined. The instrument signals were tuned using NIST614 to achieve optimal testing conditions, and the laser ablation parameters were set, including a spot size of 30 μm and an ablation frequency of 3 Hz. In this study, 100 zircon grains from each sample were randomly selected for analysis to ensure that the results accurately reflect the provenance characteristics. For the selected ablation sites, every eight sites were interspersed with a set of standards for data calibration. The standards included the international standard zircons NIST610, 91500, and PLE. The data were processed using Iolite software for baseline correction and blank subtraction to generate the final dataset. Age calculations and plot generation were then performed using Isoplot 4.15 software. The $^{207}Pb/^{206}Pb$ age is used when zircon age is higher than 1000 Ma, and the $^{206}Pb/^{238}U$ age is used when zircon age is lower than 1000 Ma. When screening the valid data, the ratio of $^{206}Pb/^{238}U$ and $^{207}Pb/^{235}U$ is used as the selection criteria, and the compatibility degree greater than 90% is the valid data. Invalid data will not be considered in this study.

To avoid a simplistic visual classification of zircon age distributions, this study plans to analyze the correlation of age populations among different samples to achieve a more refined classification. A comparative analysis of the zircon U-Pb age data from each sample was conducted using the Kolmogorov-Smirnov (K-S) non-parametric test, based on statistical principles, to reveal differences between samples from different stratigraphic levels. The Kolmogorov-Smirnov (K-S) test is a statistical method that first constructs cumulative probability curves for the zircon U-Pb age data of different datasets. The degree of correlation between the samples is then reflected by calculating the P-value (correlation coefficient). When $P \leq 0.001$, it means that there is a significant difference between the two sample age datasets; when $0.001 < P \leq 0.05$, it means that the difference between the two datasets is not significant; when $P \geq 0.05$, it indicates that there is no significant difference between the two datasets, suggesting that the two samples are highly likely to originate from the same population.

4. Results

4.1. Origin of detrital zircon

The external morphology, internal structure and Th/U ratio of detrital zircon can reflect the origin of zircon and indicate whether it has undergone long distance transportation (Fig. 3). In this study, a total of six samples comprising 600 detrital zircon grains were selected for U-Pb isotopic age analysis. Data with discordance greater than 10% and ages younger than the stratigraphic age were excluded (the stratigraphic age is determined through early seismic data and paleontological data from the oilfield), 542 zircons with concordant ages were retained for further analysis. In terms of external morphology, the six sample groups are generally similar, with grain sizes ranging from 50 to 350 μm and aspect ratios of approximately 1:1 to 1:5. Most of the zircons exhibit angular to sub-angular shapes, with a smaller portion showing sub-rounded to rounded shapes. The presence of angular zircons indicates short-distance transport, leading us to infer that the Paleozoic strata in the study area were primarily deposited through proximal sediment transport. From the perspective of internal structure characteristics of zircons, most of the zircons in this experiment can be seen with obvious oscillating zonings, which are episodic growth phenomena caused by differences in fluid composition at different stages during the zircon crystallization process. The oscillating zonings usually represent magmatic origin and are different from the cloud zonings caused by metamorphism (Corfu et al., 2003; Hanchar and Rundnick, 1995; Hoskin and Black, 2000). In addition, the ratio of Th and U content in detrital zircons can also be used to determine the origin of zircons, among which the Th/U ratio of magmatic zircons is generally higher than 0.1, and the Th/U ratio of metamorphic zircons is generally less than 0.1 (Fig. 4). Among the 542 concordant detrital zircon samples, none had a Th/U ratio of less than 0.1. Combined with the analysis of the internal structural features and Th/U ratios mentioned above, our zircon samples are characteristic of magmatic origin. The U-Pb ages of individual zircons indicate their crystallization time during magmatic activity. Therefore, the results of this zircon dating should correspond well with the tectonothermal events in the interior of the Tarim Basin and the surrounding regions of Tarim during geological history.

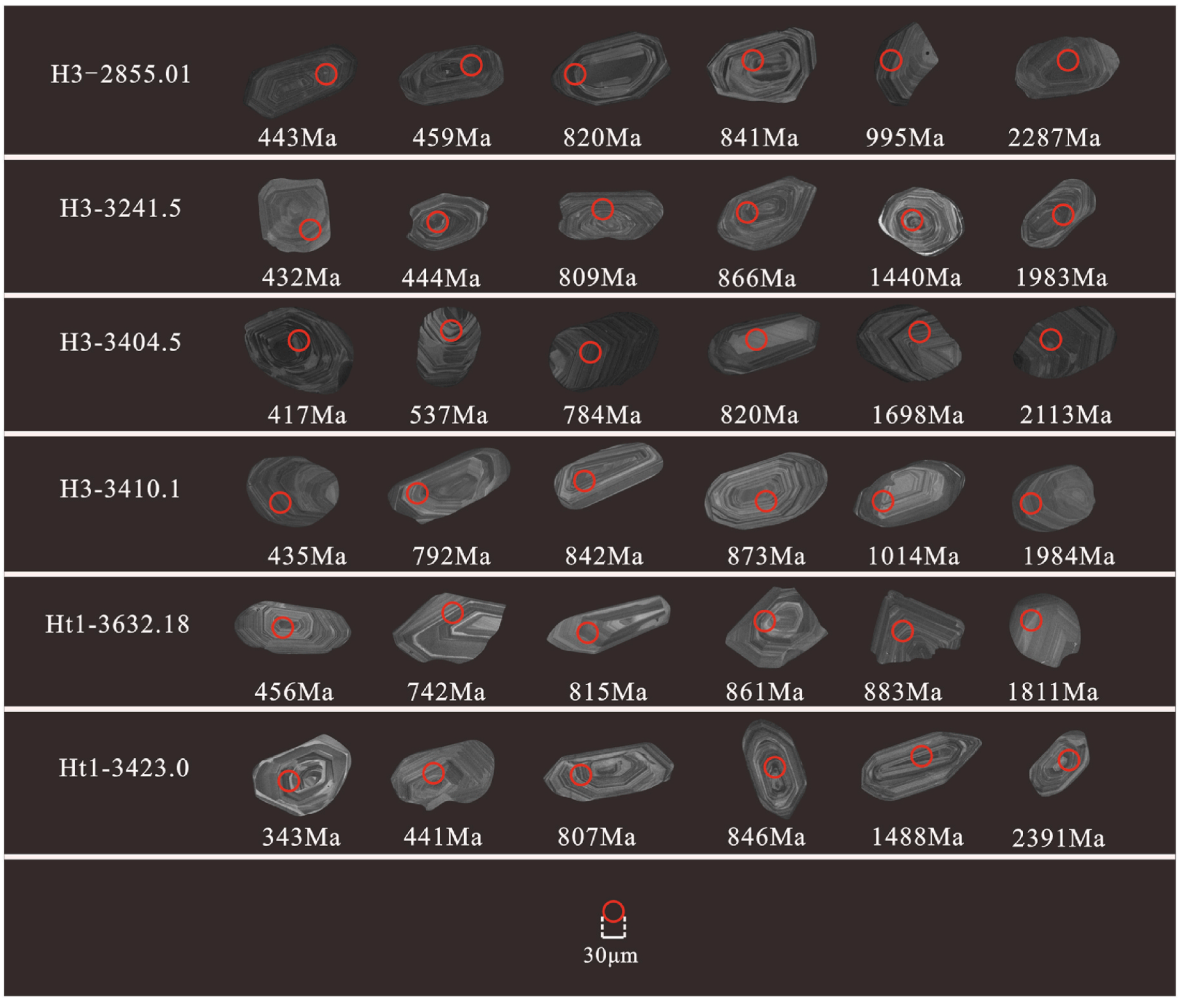

Fig. 3. Representative zircon grains from each sample in this experiment.

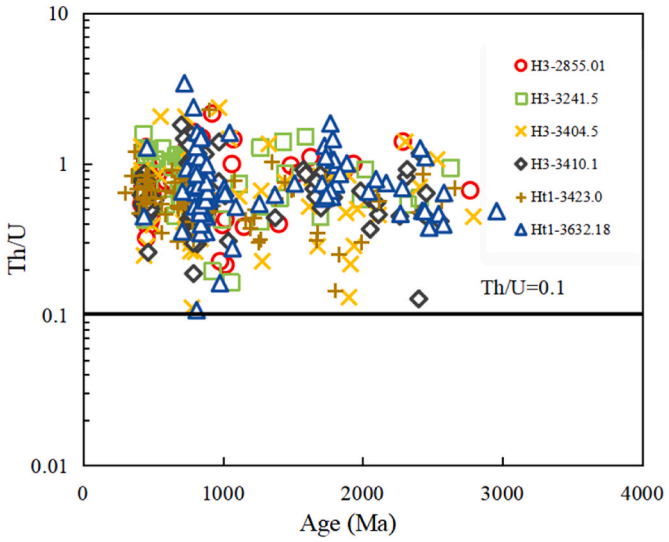

Fig. 4. Th/U versus age concordia diagram for each zircon grain.

4.2. U-Pb age of detrital zircon

4.2.1. Silurian samples

The four Silurian samples were H3-2855.01, H3-3241.5, H3-3404.5 and H3-3410.1. Samples H3-2855.01 produced a total of 94 homonic zircon ages, and identified three major age groups, namely 414-500Ma, 590-1200Ma, and 1300-2768Ma. The nuclear density estimate map produced two major peaks at 457Ma and 83 Ma. Samples H3-3241.5 produced a total of 76 harmonic zircon ages, which can be divided into three main age groups, namely 417-490Ma, 510-1300Ma and 1400-2626Ma. The probability density estimate map produced three main peaks at 438Ma, 715Ma and 806Ma. Samples H3-3404.5 produced a total of 97 harmonic zircon ages, which can be divided into three major age groups, namely 413-560Ma, 710-840Ma and 970-2792Ma. The probability density estimate map produced two major peaks at 421Ma and 795Ma. Sample H3-3410.1 produced a total of 98 harmonic zircon ages, which can be divided into three major age groups, namely 412-520Ma, 700-1100Ma and 1300-2553Ma. The probability density estimate map produced three major peaks at 422Ma and 791Ma (Figs. 5 and 6).

4.2.2. Devonian samples

The Devonian sample was Ht1-3632.18. Samples Ht1-3632.18 produced a total of 93 homonic zircon ages, and identified two major age groups, namely 433-1100Ma and 1200-2958Ma. The number of zircons in the two age groups is 62 and 31, accounting for 66.7% and 33.3%, respectively. The estimated nuclear density map produced a main peak at 836Ma (Figs. 5 and 6).

4.2.3. Carboniferous samples

The carboniferous sample is Ht1-3423.0. A total of 84 harmonic

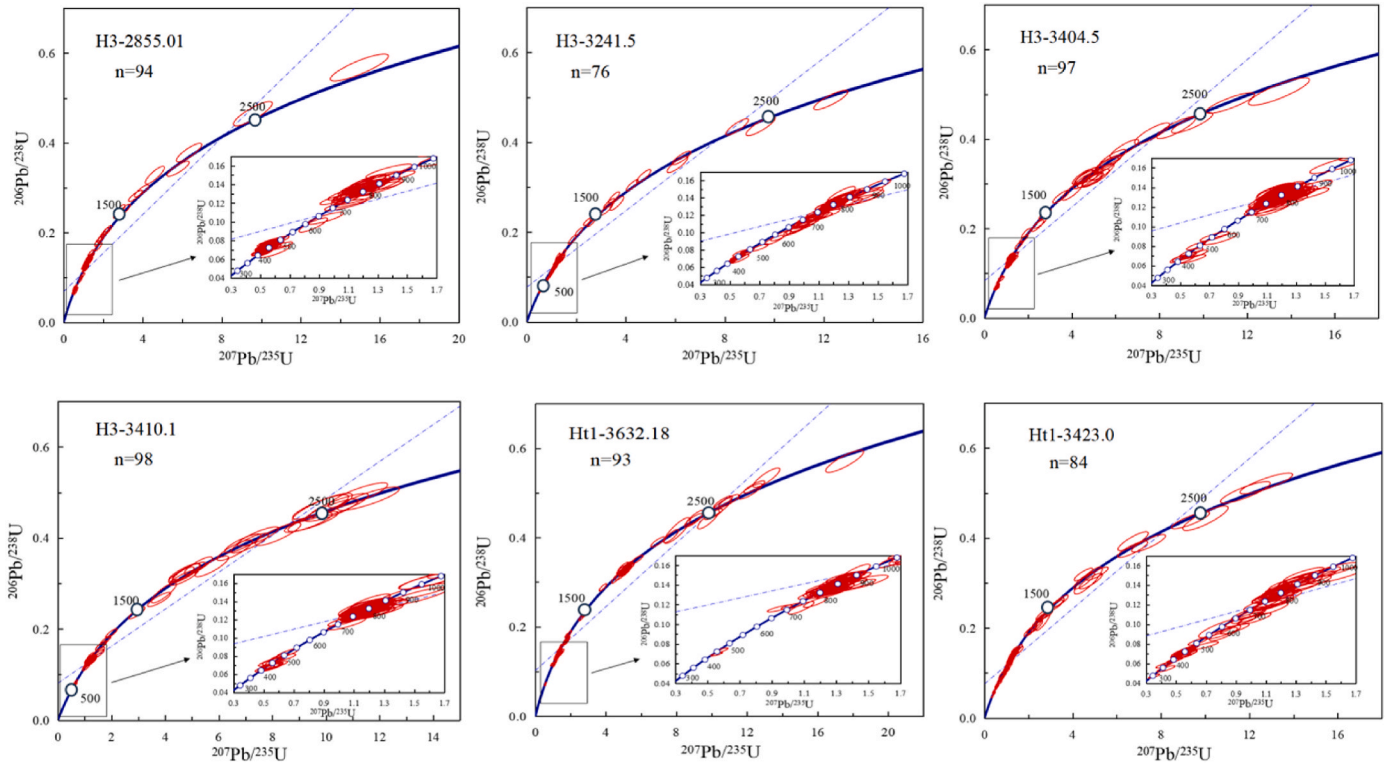

Fig. 5. Zircon U-Pb concordia diagrams in the Tarim central uplift zone.

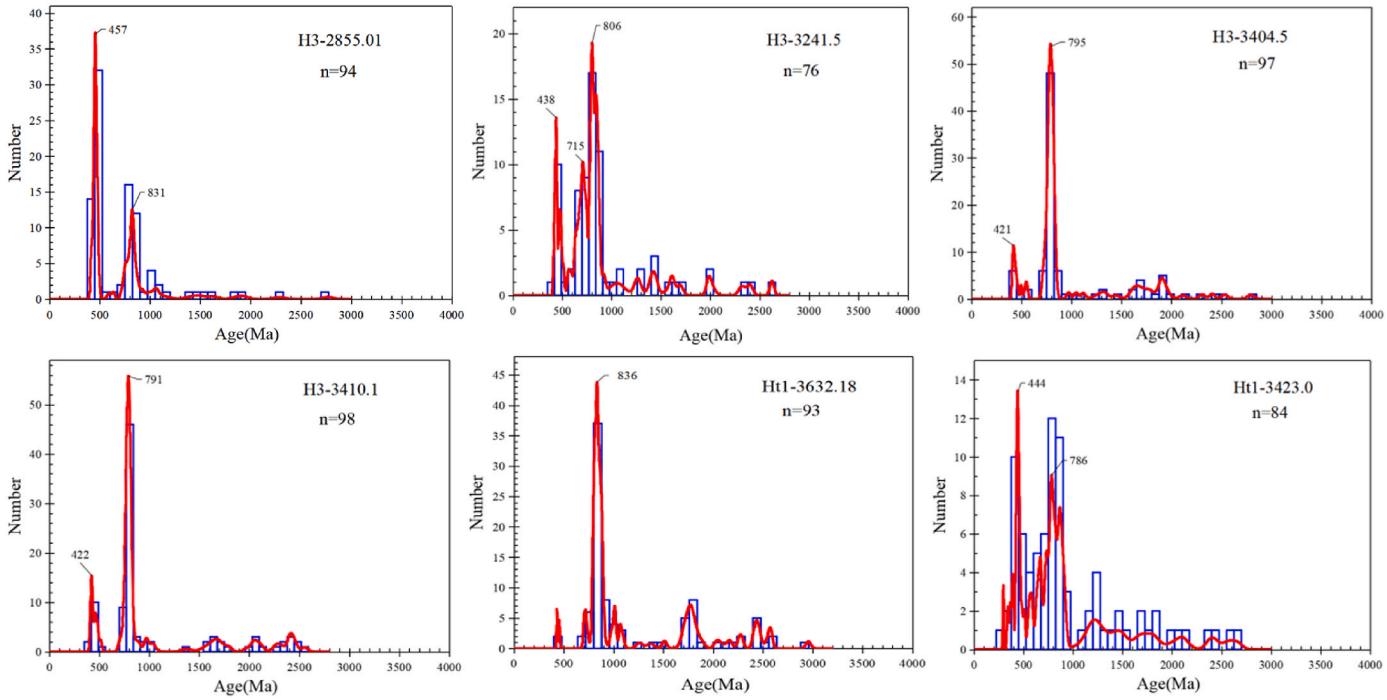

Fig. 6. Histograms and normalized probability curves of ages of detrital zircons.

zircon ages were obtained from sample Ht1-3423.0, and three major age groups were identified, namely 297-490Ma, 510-930Ma and 1080-2655Ma. The proportion of zircons in the three age groups was 21.4%, 50% and 28.6%, respectively. The kernel density estimate map produces two main peaks at 444Ma and 786Ma (Figs. 5 and 6).

4.3. K-S test results

The primary objective of this K-S test is to examine the variability between samples, allowing for further inferences on the tectonic evolution during key Paleozoic periods based on differences in provenance across various Paleozoic stages (Table 1 and Fig. 7). The K-S test results indicate a strong similarity among three of the four Silurian samples-H3-

Table 1
Results of the Kolmogorov-Smirnov test (P values) between the analyzed samples.

	Ht1-3423.0	Ht1-3632.18	H3-2855.01	H3-3241.5	H3-3404.5	H3-3410.1
Ht1-3423.0		0.000	0.001	0.327	0.003	0.004
Ht1-3632.18	0.000		0.000	0.000	0.000	0.000
H3-2855.01	0.001	0.000		0.000	0.000	0.000
H3-3241.5	0.327	0.000	0.000		0.009	0.009
H3-3404.5	0.003	0.000	0.000	0.009		0.751
H3-3410.1	0.004	0.000	0.000	0.009	0.751	

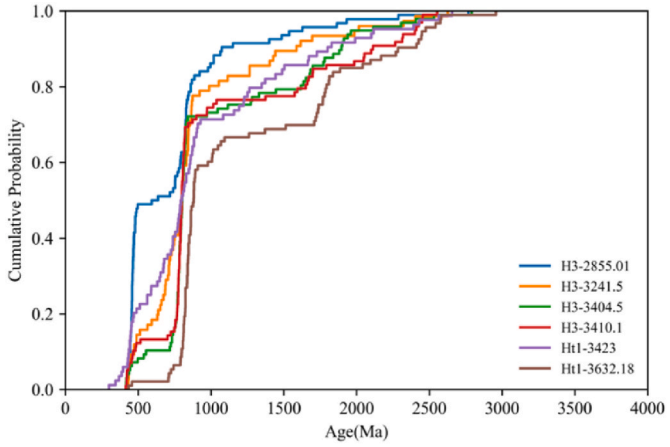

Fig. 7. Cumulative probability density plots for the different sandstone samples.

3241.5, H3-3404.5, and H3-3410.1-suggesting that their provenance likely originated from the same region. This also implies that no major tectonic deformation occurred within the Tarim Craton during this period that would have altered the provenance in the central region. Another Silurian sample, H3-2855.01, was cored from a vertical position over 400 m away from the other three samples. It shows some similarity with the data set of the Carboniferous sample Ht1-3423.0 but lacks correlation with the other three Silurian samples. The Devonian sample Ht1-3632.18 displays no correlation with any other samples, suggesting from a statistical perspective that a substantial change in provenance occurred at this time, possibly indicating a major orogenic event within or along the basin margins. The Carboniferous sample Ht1-3423.0 shows no correlation with the Devonian sample but has p-values greater than 0.001 with all Silurian samples. Notably, its p-value with H3-3241.5 reaches 0.327, suggesting a likely shared provenance between the two. It is also noteworthy that H3-2855.01, the youngest Silurian sample in this study, exhibits distinct differences from the other samples, similar to the Devonian sample. From a statistical point of view, we infer that the major tectonic changes in the central uplift zone of the Tarim Basin during the Devonian may have initiated as early as the Silurian.

5. Discussion

5.1. Zircon age and regional tectonic heat events

In this study, a total of 542 detrital zircons with concordant ages were obtained, displaying a wide U-Pb age range from 2958Ma to 297Ma. This suggests that the samples capture multiple tectonothermal events spanning from the Archean to the Paleozoic. The Archean zircons (2958-2500Ma) correspond to the formation age of the ancient basement of the Tarim Crton (2800-2500Ma). Magmatic records from this period have been found in the Kuruktag, West Kunlun, and Altyn regions of the Tarim Basin (Long et al., 2010; Zong et al., 2013; He et al., 2014). We hypothesize that the Archean zircons from the central uplift zone in this study originated from these three regions. Zircon ages ranging from 2500Ma to 2000Ma represent widespread magmatic activity within the ancient basement of the Tarim during the early Paleoproterozoic. These magmatic events, identified in the southwestern Tarim region, signify the growth of the cratonic core (Zhang et al., 2003a,b). During the Middle to Late Paleoproterozoic (2000-1500Ma), the Tarim Basin underwent collisional orogenic events, which may be associated with the assembly and breakup of the Columbia supercontinent. Several researchers have obtained age data from Tarim indicative of tectonothermal events during this period (Xin et al., 2011; Wang et al., 2017; Yang et al., 2018; Zhang et al., 2018; Cai et al., 2020). Beyond the data mentioned in Section 2 (Geological settings) above, Xin et al. (2011) found 1.87Ga of quartz syenite with A-type granite characteristics in the Altun area, southeast margin of the Tarim Basin, indicating that the Tarim Basin was in a state of extension at this time. Wang et al. (2017) discovered A-type granite with an intrusion age of 1.73Ga in the Altun area and speculated that it was the product of large-scale rifting in the late Paleoproterozoic of the Tarim Basin. Cai et al. (2020) obtained ages of 2.0–1.9 Ga for metamorphic rocks in the central Tarim region and suggested that these rocks are related to the amalgamation of the Tarim Basin with the Columbia supercontinent. Overall, a certain number of igneous rock outcrops from this period have been discovered in the Tarim Basin. Considering the global collisional events occurring during the Paleoproterozoic (2.1-1.8Ga) (Zhao et al., 2002; Santosh et al., 2006), we infer that the Paleoproterozoic zircons after 2.0Ga in this study primarily derive from volcanic records within the Tarim Basin related to the Columbia supercontinent, with the possibility of additional contributions from zircons originating in other global regions.

There is a general lack of mesoproterozoic event records in the Tarim Basin and its surrounding areas, during which the Tarim Craton was widely subjected to passive continental margin deposition. Previous studies have identified very few ages of magmatic rocks from the Mesoproterozoic, with most of them concentrated in the early Mesoproterozoic. Zhang et al., 2018 found a 1.55Ga diabase in the Kuruktag area and suggested that the diabase formed in an intraplate tension environment, which coincided with the breakup time of the Columbia supercontinent. Wang et al., 2017 discovered diabase with an age of 1497 Ma in the northern Tarim and interpreted it as originating from a rift environment. Zhang et al. (2003) determined the age of 1.2Ga of the Liancat Group igneous rocks in southwest Tarim by means of Sm-Nd isochron, and Zhang et al. (2007) also determined the age of 1.05Ga of metamorphic amphibole in this area by $^{40}Ar/^{39}Ar$. In this experiment, a small number of zircon ages were distributed between 1500 and 1000 Ma, corresponding to the relatively few tectonic events in the Tarim

Basin during this period. It is worth noting that the absence of zircon ages between 1.3Ga and 1.0Ga within the basin raises ongoing debate in the academic community regarding whether the Tarim Basin participated in the Rodinia supercontinent assembly. The existence of a Grenville orogen within the basin remains a mystery.

All the detrital zircon samples in this experiment have peak values around 800Ma, which corresponds to the widely existing magmatic records in and around the Tarim Basin studied by predecessors (Zhang et al., 2006, 2012; Xu et al., 2009), we speculate that the Tarim Basin participated in the breakup of the Rodinia supercontinent. During the Paleozoic, the Tarim Basin was formed between the West Kunlun Ocean, the Altun Ocean and the South Tianshan Ocean. With the continuous subduction and orogeny of the three ocean basins in the Paleozoic and the Tarim Craton, a large number of crystalline rocks associated with the subduction and closure of the ocean basins were produced (Wei et al., 2002; Wu et al., 2010; Wang et al., 2013; Zhang et al., 2019), the zircons analyzed in this study originated from this source.

5.2. The connection between the tarim plate and the Rodinia supercontinent

Rodinia supercontinent is another supercontinent after Colombia supercontinent. Due to its relatively complete record of sedimentary rocks, metamorphic rocks and magmatic rocks, the study of geological events related to the assembly and breakup of Rodinia supercontinent has become a hot spot of geological research worldwide (Ge et al., 2014; Zhao et al., 2021; Zhou et al., 2021). The relationship between the Tarim Craton and the Rodinia supercontinent has long been controversial.

5.2.1. Whether there is grenville orogenic belt on the tarim plate

The Grenville orogeny created one of the largest orogenic belts in geological history, known as the Grenville orogenic belt. This orogeny refers to the mountain-building events caused by the collision of landmasses during the assembly of the Rodinia supercontinent, which stitched together a series of continental blocks and microcontinents to form the supercontinent of Rodinia. Therefore, the determination of the Grenville orogenic event is considered to be direct evidence of the involvement of continental blocks in the gathering of the Rodinia supercontinent. The Tarim Craton, a major land mass in Central Asia, is considered to be a component of the Rodinian supercontinent. Scattered magmatic records around the Tarim Craton, dating to approximately 1.05-0.9Ga, have been interpreted as evidence of the Grenvillian event. However, many of these ages require further validation. For instance, Li et al. (2003) obtained an age of 932Ma from a granite sample in a well from the Tazhong uplift, which has been cited by numerous researchers as evidence of Grenvillian activity in the Tazhong uplift (Xu et al., 2013; Zhang et al., 2016; Wen et al., 2018). However, subsequent zircon dating by Wu et al. (2009) on a sample from the same well core yielded an age of 757Ma, contradicting earlier conclusions.

Zircon is typically abundant in magmatic rocks with high silica content, such as granite and granodiorite. The processes of crustal thickening and partial melting during collisional orogeny and post-collisional phases are primary mechanisms for the formation of these acidic to intermediate-acidic magmas. In contrast, during oceanic crust subduction phases and periods of plate extension and rifting, magmatic activity-such as that associated with island arc volcanism-also occurs; however, these magmas are predominantly basaltic, with limited zircon crystallization (Niu et al., 2021). Therefore, collisional orogenic events are often accompanied by extensive synchronous magmatic activity, generating substantial volumes of intermediate to acidic magmatic rocks and abundant zircon crystals, thus providing a source for surrounding areas. Such events typically leave distinct age peaks in detrital zircon records within sedimentary rocks (Hawkesworth et al., 2009). Assessing orogenic belt models through detrital zircon age peaks has thus become a common approach (Rainbird et al., 1992; Gehrels, 2014). It is undeniable that, in certain cases, compressional mechanisms induced by continental collision may inhibit magmatic activity. This inhibition typically occurs because sustained collision leads to lithospheric thickening, which increases resistance to ascending magma and hinders its ability to reach the surface. The aim of this study is to conduct a preliminary identification of tectonic events from a geochronological perspective; therefore, we have not accounted for such cases in this analysis. Globally, the Grenvillian orogeny typically leaves significant detrital zircon records in surrounding regions, as observed in eastern North America (Clay et al., 2021), southwestern North America (Howard et al., 2015), northern Scotland (Krabbendam et al., 2017), and eastern Canada (Gower et al., 2008). Consequently, if a major Grenvillian event occurred in central Tarim, by analogy, we would expect to find similar records in the extensive detrital deposits of the Tarim Basin.

This study collected published Neoproterozoic detrital zircon data from northern and southern Tarim, along with Paleozoic data obtained from central Tarim in this experiment, yielding a total of 2155 detrital zircon U-Pb age data points. On the whole, the zircon data of Southern Tarim, Central Tarim and Northern Tarim all form the major peaks in the 900-700Ma range, which is not corresponding to the Grenville orogeny event in the 1300-900Ma range, and the 900-700Ma peak is located in the period of transition from the Rodinian supercontinent to Gondwana continent (Fig. 8). Therefore, based on the statistical results of the age data, we conclude that the impact of the Grenvillian continent-continent collisional orogeny on the Tarim Craton was quite limited.

5.2.2. Collage time of north and South Tarim terranes

The above research indicates that during the Grenvillian orogeny (1.3-0.9Ga), the Tarim Basin lacks zircon geochronological records. Consequently, the timing of continent-continent collision and amalgamation of the north and south Tarim terranes also falls outside the timeframe of the Grenvillian event. In summary, scholars currently hold two main perspectives regarding the timing of the amalgamation of the north and south Tarim terranes. The first suggests that the amalgamation occurred between 2000Ma and 1900Ma. The primary evidence supporting this view is the discovery of a series of 2.0-1.9Ga igneous rocks south of the central high magnetic anomaly zone in the Tarim Basin's basement, leading to the hypothesis that during this period, the north Tarim terrane subducted towards and eventually collided with the south Tarim terrane (Yang et al., 2018; Wu et al., 2020). The second perspective posits that the amalgamation of the north and south Tarim terranes occurred between 900Ma and 700Ma, a view supported by a group of scholars. Representative data presented by Zhao et al. (2021) indicate a latitudinal difference of 28° between northern and southern Tarim around 900Ma, suggesting that an ocean still separated the north and south Tarim terranes at that time.

The first perspective does not hold up based on our data analysis. There are only 18 zircons with ages between 2000 and 1800Ma, of which only 7 fall within the 2000-1900Ma range, far fewer than the 142 zircons aged between 900 and 800Ma. Given that we expect tectonic amalgamation to manifest as prominent peaks in detrital zircon records, it is unsuitable to attribute the assembly of the Columbia supercontinent as the timing for the amalgamation of the north and south Tarim terranes The second idea, according to the results of this study, is a more appropriate interval. Igneous rocks in this region are widely developed in the Tarim Basin. Previous studies suggest that the disintegration of the Tarim Basin from the Rodinia supercontinent is a episodic process, which can be divided into four stages. The first two periods were concentrated in 820-800Ma and 780-760Ma respectively, and the main rock types were ultramafic and ferromagnesic melange, A-type granite, and basic dike groups distributed in Aksu and West Kunlun areas (Long et al., 2011; Zhang et al., 2011), the third stage is 740-735Ma, mainly bimodal intrusive rocks distributed in the Kuruktag area (Xu et al., 2009; Zhang et al., 2013); The fourth stage is 650-635Ma, which mainly represents rock types including basic dike group, andesite and potassic granite (Zhu et al., 2008). Scholars interpret the magmatic rocks in these four stages as the products of continental rifting, and propose that they

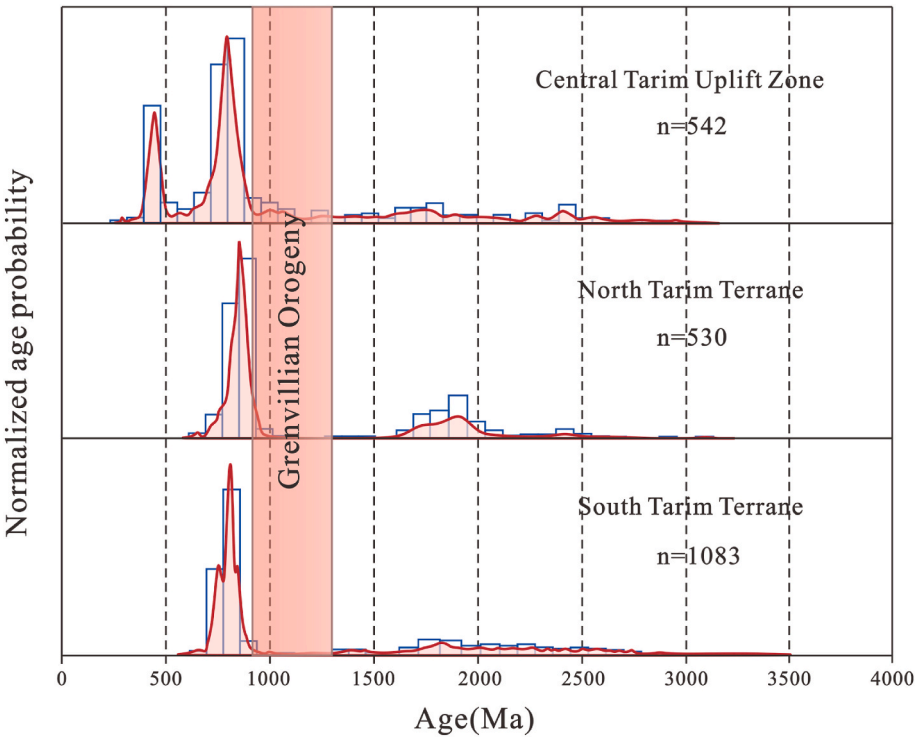

Fig. 8. Age spectra of detrital zircons in three major terranes of Tarim Basin. North Tarim Terrane (Wu et al., 2018; Ding et al., 2015; Sun et al., 2022); South Tarim Terrane (Wang et al., 2015, 2020; Wang et al., 2020a,b).

may be related to the multi-stage mantle plume related to the breakup of the Rodinia supercontinent (Zhu et al., 2008; Xu et al., 2009; Long et al., 2011; Zhang et al., 2011, 2013). Therefore, after 820 Ma, the tarim is in a rift environment, which may represent a state of extension, so there is no possibility of plate collision at this stage. Based on previous research, we propose a model for the amalgamation of the northern and southern Tarim, suggesting that the south Tarim terrane, central Tarim, and north Tarim terrane amalgamated between 900Ma and 820Ma, followed by the influence of mantle plume upwelling during the breakup of Rodinia between 820Ma and 600Ma (Fig. 9). It is worth noting that this model is similar to the widely accepted "collision-breakup model" of the Tarim

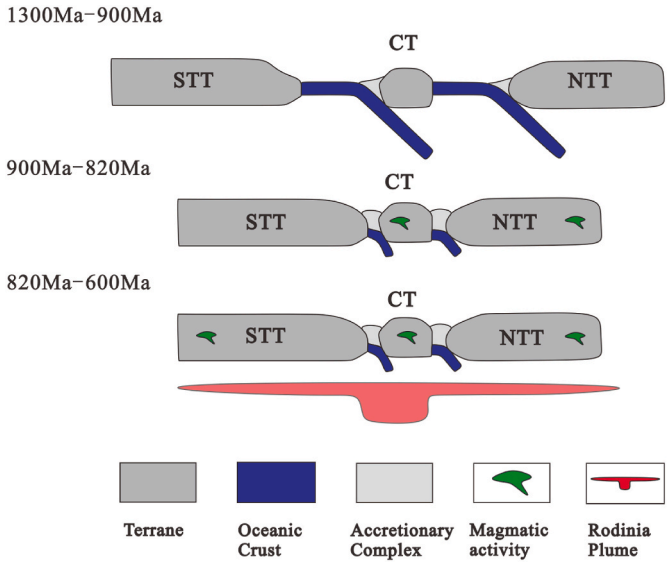

Fig. 9. Collage pattern of North and south Tarim terranes (modified after Zhang et al., 2024). Note: NTT, North Tarim terrane; STT, South Tarim terrane; CT, Central Tarim terrane.

block's relationship with the Rodinia supercontinent proposed by earlier scholars (Xu et al., 2013; Zhang et al., 2016). This model suggests that the south Tarim terrane amalgamated with northern Australia during the late Mesoproterozoic to early Neoproterozoic via a "Grenvillian" orogenic belt. Subsequently, between 900 and 820Ma, it joined with the north Tarim terrane along the Tazhong suture during the mid to late Neoproterozoic. Magmatic activity in Tarim after 820Ma is thus interpreted by this model as a product of the breakup of the Rodinia supercontinent. However, unlike previous models, our model does not suggest that the south Tarim terrane amalgamated with Australia during the Grenvillian orogeny; rather, it was likely located on Australia's periphery. Based on the presence of 800Ma magmatic rocks along the northern margin of Tarim, indicative of subduction, we infer that both the north and south Tarim terranes were situated on the outskirts of the Rodinia supercontinent. The northern side of Tarim faced the Pan-Rodinia Ocean, experiencing prolonged subduction, which aligns with Ge's "long-term subduction-accretion orogeny" model (Ge et al., 2014, 2016). As for the specific dynamics of the north and south Tarim amalgamation, our data cannot fully address this question. However, based on previous studies, we speculate that unidirectional subduction of oceanic crust existed between the north and south Tarim terrane (Zhao et al., 2021).

5.3. Paleozoic basin-mountain relationship and tectonic evolution of the central uplift zone

During the Neoproterozoic, the Tarim Basin developed into an independent and stable craton. Therefore, the source-sink system and the plate tectonic environment of the basin during the Paleozoic sedimentation in the central uplift zone are closely related to the subduction, reduction, and collision processes of the Proto-Tethys Ocean to the southwest, the Altyn Ocean to the southeast, and the Tianshan Ocean to the north. We compiled published detrital zircon data from sedimentary rocks in the West Kunlun orogenic belt, northern Tarim, and South Tianshan, along with published intermediate-acidic magmatic rock data

from the West Kunlun, Altyn, and South Tianshan orogenic belts, and compared these with our detrital zircon data (Fig. 10). Given that the detrital zircon ages obtained in this experiment are predominantly older than 400Ma (except for Carboniferous sample Ht1-3423.0), our analysis focuses primarily on tectonic activity in the surrounding orogenic belts during the 600-400 Ma interval.

First, we need to identify the provenance of our detrital zircons. All six samples exhibit a prominent age peak around 800Ma, which aligns only with detrital zircon samples from north Tarim. In contrast, detrital zircons from the Paleozoic and older periods are scarce in the South Tianshan and West Kunlun orogenic belts, rendering them insufficient as the primary source for the samples in this study. As mentioned earlier, the Tarim Basin was involved in the breakup of the Rodinia supercontinent around 800Ma. Previous studies have reported a series of bimodal volcanics (Zhu et al., 2008), S-type granites (Deng et al., 2008), and granites in the Kuruktag area (Ge et al., 2014) from this period. These magmatic rocks likely contain abundant zircons, serving as potential sources for our samples. We also observed distinct age peaks between 600Ma and 200Ma in three samples, H3-2855.01, H3-3241.5, and Ht1-3423.0, with other samples containing zircons from this age range as well. Since there is no evidence of magmatic activity within Tarim during this period, these zircons likely originated from the surrounding orogenic belts. However, given their relatively low abundance, they cannot be considered the primary source for these samples; instead, the primary provenance is likely to be the interior of the Tarim Basin and the interaction between the Tarim Basin and the surrounding orogenic belts.

Existing data indicate that magmatic rock ages in the Altyn orogenic belt are primarily distributed across four intervals: 520-477Ma, 460-440Ma, 430-380Ma, and 360-320Ma. Kang et al. (2011) measured a U-Pb zircon age of 500.3Ma for granites along the northern margin of the Altyn tectonic belt and attributed their formation to a continental margin volcanic arc environment associated with oceanic crust subduction. Han et al. (2012) dated exposed volcanic rocks in the Kaladawan area of Altyn to between 485 and 477Ma, a range similar to that obtained by Chen et al. (2016) interpreting this as an island arc tectonic setting on an active continental margin. Hao et al. (2006) obtained ^{40}Ar-^{39}Ar ages of 455Ma and 450Ma from ophiolitic mélanges along the northern margin of Altyn, suggesting that oceanic crust subduction in northern Altyn concluded around 450Ma. Wu et al. (2007) identified granites with S-type characteristics and an age of 440Ma in northern Altyn, indicating that subduction and collision in the northern Altyn Ocean occurred prior to 440Ma. Wu et al. (2016) obtained multiple magmatic ages of 411-404Ma and 352-343Ma in the southern Altyn region, attributing these to post-collisional orogenic equilibration and Tethyan tectonic activity, respectively. The closure of the Proto-Tethys Ocean, marked by the Kudi ophiolitic mellitic belt in the West Kunlun, occurred later than that of the Altyn Ocean (Yuan et al., 2002; Zhang et al., 2018, 2020; Wang et al., 2020a,b). Zhang et al., 2018 measured a 530Ma gabbro in the eastern Pamir Plateau, proposing that initial subduction of the Proto-Tethys Ocean began around 540-530Ma, while evidence discovered by Zhang et al. (2020) in the South Kunlun terrane (rhyolite at 519-513Ma) suggests that subduction likely commenced prior to 520Ma. Previous studies, considering the presence of 420-405Ma A-type granites in Kudi formed in an intraplate extensional setting and the results of detrital zircon dating, inferred that the closure of the Proto-Tethys Ocean between the South Kunlun terrane and the Tarim Craton occurred between 431Ma and 420Ma (Yuan et al., 2002; Wang et al., 2020a,b). Overall, the West Kunlun orogenic belt

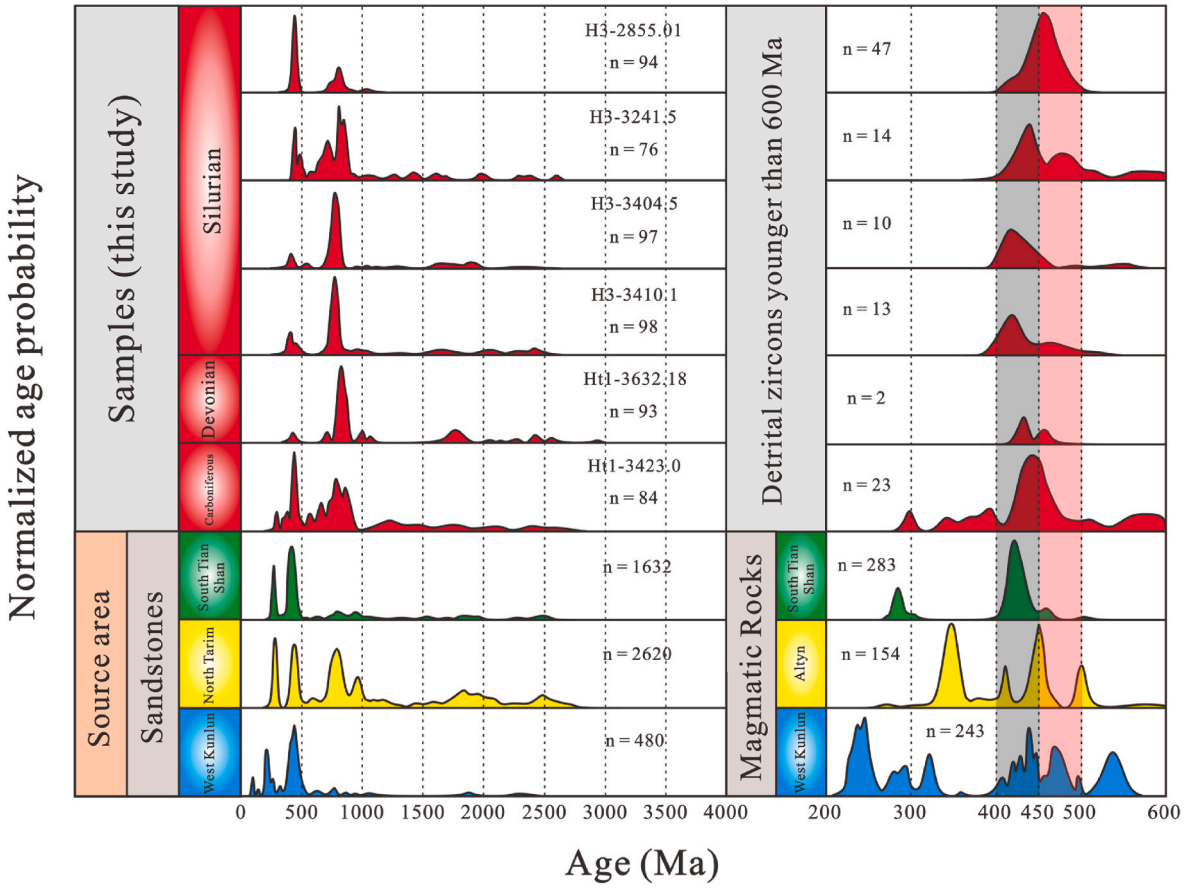

Fig. 10. Zircon age comparison diagram. Detrital zircons in sedimentary rocks: South Tianshan (Wang et al., 2018); North Tarim (Wang et al., 2018); West Kunlun (Blayney et al., 2016; Gao et al., 2024). Detrital zircons in magmatic rocks: South Tianshan (Li et al., 2023; Zhang et al., 2014; Guo et al., 2013; Ge et al., 2012a,b; Zhao et al., 2015); Altyn (Kang et al., 2011, 2013; Wu et al., 2016); West Kunlun (Sui, 2021; Kang et al., 2015; Chen et al., 2020; Wei, 2018; Allen et al., 2023).

experienced sustained and intense magmatic and tectonic activity between 500Ma and 400Ma. There was oceanic subduction to the south in the central Tianshan area during the Silurian period, while the South Tianshan Ocean had not yet opened, leaving the northern margin of the Tarim Basin without conditions for large-scale orogeny or erosion. Correspondingly, the Paleozoic crystalline rock ages in the South Tianshan and Central Tianshan orogenic belts are mostly younger than 460Ma, aligning with the 460-400Ma granite intrusions identified in the Harke and Kuruktag regions at the intersection of the South Tianshan and Tarim (Lin et al., 2013; Guo et al., 2013; Ge et al., 2012a,b; Zhao et al., 2015; Dong et al., 2016).

A comprehensive analysis of the six samples from this experiment shows consistent age distributions between 500Ma and 400Ma across all samples. We can confidently identify the magmatic rocks of the West Kunlun orogenic belt as a source for the samples from central Tarim, as it is the only region with evidence of significant magmatic activity around 480Ma. Similarly, only the 450Ma peak age of magmatic zircons from the Altun Mountains corresponds to the 450Ma peaks of H3-2855.01 and Ht1-3423.0. Additionally, only the magmatic rock ages around 350Ma from the Altun Mountains align with the zircon ages in the Carboniferous Ht1-3423.0 at this stage. Therefore, the magmatic rocks from the Altun Mountains also contributed to the provenance of the central Tarim Basin. Based on the zircon ages around 300Ma in the Carboniferous sample Ht1-3423.0, magmatic activity from the South Tianshan corresponds with it. In summary, the tectonic activities of the Altun orogenic belt, the West Kunlun orogenic belt, and the South Tianshan orogenic belt collectively influenced sedimentation in the central Tarim Basin. According to the K-S test results, a distinct shift exists among the six samples, specifically indicating that the Devonian sample Ht1-3632.18 and the youngest Silurian sample H3-2855.01 show no correlation with the other samples. Combined with our petrographic observations, it is evident that H3-2855.01 experienced a notable provenance change, potentially extending into the Devonian period. This is plausible, as during the Late Silurian, major magmatic intrusions were occurring in the South Tianshan, West Kunlun, and Altun regions. These regions collectively compressed the Tarim Craton from different directions, and this compression likely transmitted to the central Tarim Basin either concurrently or shortly afterward, resulting in a shift in the central Tarim provenance. The primary Paleozoic provenance in the central Tarim Basin can be reasonably attributed to magmatic rocks within Tarim, corresponding to the breakup period of the Rodinia supercontinent. The combined compressive forces from the three major orogenic belts extensively exposed and eroded the 900-700Ma granitic outcrops in Tarim, as evidenced by the widespread distribution of Neoproterozoic granites in regions such as Kuruktag in north Tarim (Ge et al., 2014).

5.4. Significance in petroleum geology

By determining the regional paleogeographic conditions at specific times through detrital zircon dating, an initial understanding of hydrocarbon source rock enrichment and migration systems can be obtained. The optimal environment for organic matter enrichment is found in depressions formed under extensional and subsidence conditions (Demaison and Moore, 1980; Wu et al., 2025). The primary reasons are as follows: first, subsiding regions enable the rapid accumulation of thick sediment layers, promoting the quick burial and preservation of organic matter. Second, these regions often form lake environments with anoxic, reducing conditions that further aid in organic matter preservation. Third, due to the greater sediment depth typical of extensional areas, organic matter can more readily enter the oil-generating window under high-temperature and high-pressure conditions. In contrast, the sediments in the uplifted areas undergo relatively poor compaction, making it difficult for the organic matter to reach conditions suitable for hydrocarbon generation.

In the central Tarim uplift, significant breakthroughs in oil and gas exploration have not been achieved in the Bachu Uplift area, which is closely related to the absence of thicker source rocks in this region. Currently, major oil and gas fields in the Tarim Basin are mainly concentrated in two sets of source rocks: the Carboniferous-Permian and the Triassic-Jurassic. The Cambrian source rocks are primarily distributed in the eastern part of the Tarim Basin and have relatively small thicknesses, generally less than 200 m (Hu et al., 2024; Wang et al., 2024). Based on the oil and gas discoveries in the Bachu area, the main source rocks are located in the middle and lower Cambrian strata, which are associated with the deposition of restricted platform lagoons. These source rocks are clearly controlled by the restricted platform depressions (Ning et al., 2021). This is closely related to the lack of major tectonic activity in the Tarim Basin during the Cambrian, as illustrated in Fig. 10. From the above conclusions, it can be observed that the Tarim Basin's surrounding orogenic belts, during the Silurian and Carboniferous, experienced continued tectonic activity, with the basin interior undergoing compressional stress and the central uplift undergoing intense deformation. As a result, deep lacustrine deposits are unlikely to have formed in the central uplift zone. Therefore, to this day, no source rock strata have been found in the Silurian to Carboniferous sequences of the central uplift zone.In the West Kunlun region, there was a period of tectonic stability between 400 Ma and 320 Ma, during which stretching effects cannot be ruled out. In some areas, the lake waters were relatively deep. Additionally, under the influence of upwelling currents and thermal water caused by rifting and basin expansion, biological development was relatively advanced. Consequently, the Carboniferous source rocks in this region are now one of the main target intervals for deep and ultra-deep exploration in the southwestern foreland of the Tarim Basin (Wang et al., 2024).

6. Conclusions

(1) The detrital zircon ages from the Silurian to Carboniferous strata in the Central Uplift of the Tarim Basin exhibit two prominent peaks, at 452Ma and 806Ma, respectively no age peaks were observed outside of these two ranges in any of the samples.
(2) The influence of the Grenville Orogeny on the Tarim Basin was very limited. The 542 Paleozoic zircon ages obtained in this study, combined with the 1613 published Neoproterozoic detrital zircon U-Pb age data from the northern and southern Tarim, do not correspond to the 1300-900 Ma Grenville Orogenic event.
(3) The suturing of the South and North Tarim terranes likely occurred between 900Ma and 820Ma. In the Paleozoic zircon age distribution of the Central Uplift, the number of zircons dated between 2000Ma and 1800Ma is significantly lower than those dated between 900Ma and 800Ma. This period of collisional orogeny contributed to the formation of a stable Tarim Craton.
(4) The central Tarim region was influenced by the combined effects of the surrounding West Kunlun, Altun, and South Tianshan orogenic belts from the Silurian to the Carboniferous. The primary provenance of the six samples analyzed in this study originates from within the Tarim Basin, as extensive erosion occurred within the basin following compressional forces from the surrounding orogenic belts. This erosion predominantly exposed magmatic outcrops from the Rodinia supercontinent breakup period.

CRediT authorship contribution statement

Yang Gao: Writing – original draft, Software, Methodology, Data curation, Conceptualization. **Lin Jiang:** Project administration, Investigation, Funding acquisition. **Weiyan Chen:** Writing – review & editing, Methodology, Conceptualization. **Hongkui Dong:** Supervision, Project administration. **Wen Zhao:** Writing – review & editing. **Fujie Jiang:** Supervision, Conceptualization. **Qingong Zhuo:** Writing – review & editing. **Haizu Zhang:** Writing – review & editing. **Yao Hu:** Data curation. **Zhou Fang:** Writing – review & editing. **Xiaohao Wang:**

Writing – review & editing. **Yingqi Feng:** Investigation.

Declaration of competing interest

The authors declare that they have no known competing financial interests or personal relationships that could have appeared to influence the work reported in this paper.

Acknowledgments

This work was supported by the Second Tibetan Plateau Scientific Expedition and Research Program (STEP), Grant No. 2019QZKK0708, and the National Natural Science Foundation of China, Grant No. U22B6002.

Appendix A. Supplementary data

Supplementary data to this article can be found online at https://doi.org/10.1016/j.marpetgeo.2025.107292.

Data availability

Data will be made available on request.

References

Allen, M.B., Song, S.G., Wang, C., Zeng, R.Y., Wen, T., 2023. An oblique subduction model for closure of the Proto-Tethys and Palaeo-Tethys oceans and creation of the Central China Orogenic Belt. Earth Sci. Rev. 240, 104385.

Blayney, T., Najman, Y., Dupont-Nivet, G., Carter, A., Millar, I., Garzanti, E., Sobel, E.R., Rittner, M., Ando, S., Guo, Z.J., Vezzoli, G., 2016. Indentation of the Pamirs with respect to the northern margin of Tibet: constraints from the Tarim basin sedimentary record. Tectonics 35 (9–10), 2345–2369.

Cai, Z.H., Jiao, C.L., He, B.Z., Qi, L.X., Ma, X.X., Cao, Z.C., Xu, Z.Q., Chen, X.J., Liu, R.H., 2020. Archean-Paleoproterozoic tectonothermal events in the central Tarim Block: constraints from granitic gneisses revealed by deep drilling wells. Precambrian Res. 347, 105776.

Carroll, A.R., Graham, S.A., Chang, E.Z., Mcknight, C., 2001. Sinian through permian tectonostratigraphic evolution of the northwestern Tarim Basin, China. Geol. Soc. Am. Mem. 194, 47–70.

Chen, B.L., Li, S.B., Jiang, R.B., Chen, Z.L., Han, F.B., Cui, L.L., Li, L., Zhao, S.M., Qi, W. X., Yang, Y., Wang, S.X., Wang, Y., Zhou, Y.G., Hao, R.X., 2016. Zircon SHRIMP U-Pb dating of intermediate-felsic volcanic rocks from the kaladawan Area,Altun mountains and its tectonic environment. Acta Geol. Sin. 90 (4), 708–727 in Chinese with English abstract.

Chen, G.M., Liu, J.C., Wang, Y.T., Hu, Q.Q., Huang, S.K., Sun, Z.H., Nijiati, A.B.D.X., Kong, D.Y., Liu, J.F., 2020. Zircon U-Pb dating and geochemical characteristics of early paleozoic granitein the southern sunake of West Kunlun,northwest chinaand their geological significances. J. Earth Sci. Environ. 2020 42 (4), 427–441 in Chinese with English abstract.

Chen, N.S., Liao, F.X., Wang, L., Santosh, M., Sun, M., Wang, Q.Y., Mustafa, H.A., 2013. Late paleoproterozoic multiple metamorphic events in the Quanji Massif: links with tarim and North China cratons and implications for assembly of the Columbia supercontinent. Precambr. Res. 228, 102–116.

Chen, W.Y., Zhu, G.Y., Zhang, K.J., Zhang, Y.J., Yan, H.H., Du, D.D., Zhang, Z.Y., Xia, B., 2020. Late Neoproterozoic intracontinental rifting of the Tarim carton, NW China: an integrated geochemical, geochronological and Sr-Nd-Hf isotopic study of siliciclastic rocks and basalts from deep drilling cores. Gondwana Res. 80, 142–156.

Clay, J.M., Moecher, D.P., Bowersox, J.R., 2021. Detrital zircon U-Pb geochronology of the precambrian middle run formation (eastern Northnorth America basement): implications for grenvillian foreland basin evolution and midcontinent rifting. Precambrian Res. 364, 106332.

Corfu, F., Hanchar, J.M., Hoskin, P.W., Kinny, P., 2003. Atlas of zircon textures. Rev. Mineral. Geochem. 53, 468–500.

Demaison, G.J., Moore, G.T., 1980. Anoxic environments and oil source bed genesis. Org. Geochem. (Tokyo. 1967) 2 (1), 9–31.

Deng, X.L., Shu, L.S., Zhu, W.B., Ma, D.S., Wang, B., 2008. Precambrian tectonism magmatiam, deformation and geochronology of igneous rocks in the Xingdi fault zone. Xinjiang. Acta Petrol. Sin 24 (12), 2800–2808 in Chinese with English abstract.

Ding, H.F., Ma, D.S., Lin, Q.Z., Jing, L.H., 2015. Age and nature of Cryogenian diamictites at Aksu, Northwest China: implications for Sturtian tectonics and climate. Int. Geol. Rev. 57, 2044–2064.

Dong, S.L., Li, Z., Jiang, L., 2016. The Ordovician-Silurian tectonic evolution of the northeastern margin of the Tarim block, NW China: constraints from detrital zircon geochronological records. J. Asian Earth Sci. 122, 1–9.

Eizenhöfer, P.R., Zhao, G.C., Zhang, J., Sun, M., 2014. Final closure of the PaleoAsian Ocean along the solonker suture zone: constraints from geochronological and geochemical data of permian volcanic and sedimentary rocks. Tectonics 33, 441–463.

Eizenhöfer, P.R., Zhao, G.C., Sun, M., Zhang, J., Han, Y.G., Hou, W.Z., 2015. Geochronological and Hf isotopic variability of detrital zircons in Paleozoic strata across the accretionary collision zone between the North China craton and Mongolian arcs and tectonic implications. Geol. Soc. Am. Bull. 127 (9–10), 1422–1436.

Eizenhöfer, P.R., Zhao, G.C., 2018. Solonker suture in east Asia and its bearing on the final closure of the eastern segment of the palaeo-asian ocean. Earth Sci. Rev. 186, 153–172.

Feng, D., Wang, C., Song, S.G., Xiong, L., Zhang, G.B., Allen, MarkB., Dong, J., Wen, T., Su, L., 2023. Tracing tectonic processes from proto-to paleo-tethys in the east Kunlun orogen by detrital zircons. Gondwana Res. 115, 1–16.

Gao, Y., Jiang, L., Chen, W.Y., Jiang, F.J., Dong, H.K., Zhao, W., Dong, C.Y., Feng, Y.Q., 2024. Provenance of cretaceous sediments in the West Kunlun piedmont belt and implications for tectonic evolutionary events. Front. Earth Sci. 12, 1431866.

Ge, R.F., Zhu, W.B., Wu, H.L., Zheng, B.H., Zhu, X.Q., He, J.W., 2012a. The paleozoic northern margin of the tarim craton: passive or active? Lithos 142–143, 1–15.

Ge, R.F., Zhu, W.B., Zheng, B.H., Wu, H.L., He, J.W., Zhu, X.Q., 2012b. Early Pan-African magmatism in the Tarim Craton: insights from zircon U-Pb-Lu-Hf isotope and geochemistry of granitoids in the Korla area, NW China. Precambr. Res. 212–213, 117–138.

Ge, R.F., Zhu, W.B., Wu, H.L., He, J.W., Zheng, B.H., 2013. Zircon U-Pb ages and Lu-Hf isotopes of Paleoproterozoic metasedimentary rocks in the Korla Complex, NW China: implications for metamorphic zircon formation and geological evolution of the Tarim Craton. Precambrian Res. 231, 1–18.

Ge, R.F., Zhu, W.B., Wilde, S.A., He, J.W., Cui, X., Wang, X., Zheng, B.H., 2014. Neoproterozoic to paleozoic long-lived accretionary orogeny in the northern tarim craton. Tectonics 33 (3), 302–329.

Ge, R.F., Zhu, W.B., Wilde, S., 2016. Mid-Neoproterozoic (ca. 830-800 Ma) metamorphic P-T paths link Tarim to the circum-Rodinia subduction - accretion system. Tectonics 35, 1465–1488.

Gehrels, G.E., 2014. Detrital zircon U-Pb geochronology applied to tectonics. Annu. Rev. Earth Planet Sci. 42, 127–149.

Gower, C.F., Kamo, S.L., Kwok, K., Krogh, T.E., 2008. Proterozoic southward accretion and Grenvillian orogenesis in the interior Grenville Province in eastern Labrador: evidence from U-Pb geochronological investigations. Precambrian Res. 165 (1–2), 61–95.

Guo, R.Q., Nijiati, A., Qin, Q., Jia, X.L., Zhu, Z.X., Wang, K.Z., Li, X.P., 2013. Geological characteristics and tectonic significance of Silurian granitic intrusions in the northern Tarim craton. Xinjiang. Geol. Bull. China, 2013 32 (2/3), 220–238 in Chinese with English abstract.

Guo, R.Q., Qin, Q., Muhetaer, Z., Zhao, L.L., Sun, M.J., Wei, Z., 2013. Geological characteristics and tectonic significance of Ordovician granite intrusions in the western segment of Quruqtagh, Xinjiang. Earth Sci. Front, 2013 20 (4), 251–263 in Chinese with English abstract.

Guo, X.C., Zheng, Y.Z., Gao, J., Zhu, Z.X., 2013. Determination and geological significance of the mesoarchean craton in western Kunlun mountains, Xinjiang, China. Geol. Rev. 59 (3), 401–412 in Chinese with English abstract.

Guo, Y., Zhao, G.C., Guo, R.Q., Han, Y.G., Liu, Q., Wei, Z., Zhou, N.C., Ju, P.C., Song, Z. H., 2022. Metamorphism and geochronology of garnet mica schists from the Kuluketage area: implications for reconstructions of the Tarim Craton in supercontinent Columbia. Precambrian Res. 379, 106806.

Guo, Y., Zhao, G.C., Guo, R.Q., Han, Y.G., Liu, Q., Zhou, N.C., Song, Z.H., 2023. Metamorphism and chronology of Paleoproterozoic mafic granulite from the Kuluketage area, northern Tarim and its tectonic applications. Precambrian Res. 393, 107092.

Guo, Z.J., Yin, A., Robinson, A., Jia, C.Z., 2005. Geochronology and geochemistry of deep drill-core samples from the basement of the central Tarim basin. J. Asian Earth Sci. 25 (1), 45–56.

Han, F.B., Chen, B.L., Cui, L.L., Wang, S.X., Chen, Z.L., Jiang, R.B., Li, L., Qi, W.X., 2012. Zircon SHRIMP U-Pb age of intermediate-acid intrusive rocks in Kaladawan area, eastern Altun Mountains, NW China, and its implications. Acta Petrol. Sin. 28 (7), 2277–2291 in Chinese with English abstract.

Hanchar, J.M., Rundnick, R.L., 1995. Revealing hidden structures: the application of cathodoluminescence and backscattered electron imaging to dating zircons from lower crustal xenoliths. Lithos 36, 289–303.

Hao, J., Wang, E.Q., Liu, X.H., Sang, H.Q., 2006. Jinyanshan collisional oroginic belt of the early Paleozoic in the Altun mountains: evidence from single zircon U-Pb and $^{40}Ar/^{39}Ar$ isotopic dating for the are magmatite and ophiolitic mélange. Acta Petrol. Sin. 22 (11), 2743–2752 in Chinese with English abstract.

Hawkesworth, C., Cawood, P., Kemp, T., Storey, C., Dhuime, B., 2009. A matter of preservation. Science 323 (5910), 49–50.

He, J.W., Zhu, W.B., Ge, R.F., Zheng, B.H., Wu, H.L., 2014. Detrital zircon U-Pb ages and Hf isotopes of Neoproterozoic strata in the Aksu area, northwestern Tarim Craton: implications for supercontinent reconstruction and crustal evolution. Precambrian Res. 254, 194–209.

He, J.Y., Xu, B., Li, D., 2019. Newly discovered early Neoproterozoic (ca. 900 Ma) andesitic rocks in the northwestern Tarim Craton: implications for the reconstruction of the Rodinia supercontinent. Precambrian Res. 325, 55–68.

Hoskin, P.W.O., Black, L.P., 2000. Metamorphic zircon formation by solid-state recrystallization of protolith igneous zircons. J. Metamorph. Geol. 18, 423–439.

Howard, A.L., Farmer, G.L., Amato, J.M., Fedo, C.M., 2015. Zircon U–Pb ages and Hf isotopic compositions indicate multiple sources for Grenvillian detrital zircon deposited in western Laurentia. Earth Planet Sci. Lett. 432, 300–310.

Hu, Y., Jia, C.Z., Chen, J.Q., Pang, X.Q., Jiang, L., Wang, C.X., Xiao, H.Y., Li, C.J., Jin, Y. J., 2024. Restoration of hydrocarbon generation potential of the highly mature Lower Cambrian Yuertusi Formation source rocks in the Tarim Basin. Petrol. Sci. 1995–8226.
Jia, C.Z., Wei, G.Q., 2002. Structural characteristics and oil-gas properties of Tarim Basin. Chin. Sci. Bull. 47 (S1), 1–8 in Chinese.
Jia, C.Z., 2009. The structures of Basin and range system around the T ibetan plateauand the distribution of oil and gas in the Tarim Basin. Geotect. Metallogenia 33 (1), 1–9 in Chinese with English abstract.
Kang, L., Liu, L., Cao, Y.T., Wang, C., Yang, W.Q., Zhu, X.H., 2011. Zircon LA-ICP-MS U-Pb ages and Hf isotopes of Hongliugou moyite from north Altyn Tagh tectonic belt. Geol. Bull. China, 2011 30 (7), 1066–1076 in Chinese with English abstract.
Kang, L., Liu, L., Cao, Y.T., Wang, C., Yang, W.Q., Liang, S., 2013. Geochemistry, zircon U-Pb age and its geological significance of the gneissic granite from the eastern segment of the Tatelekebulake composite granite in the south Altyn Tagh. Acta Petrol. Sin. 29 (9), 3039–3048 in Chinese with English abstract.
Kang, L., Xiao, P.X., Gao, X.F., Wang, C., Yang, Z.C., Xi, R.G., 2015. Geochemical characteristics,petrogenesis and tectonic seting of Oceanic plagiogranites belt in the northwestern margin of western Kunlun. Acta Petrol. Sin. 31 (9), 2566–2582 in Chinese with English abstract.
Krabbendam, M., Bonsor, H., Horstwood, M.S.A., Rivers, T., 2017. Tracking the evolution of the Grenvillian foreland basin: constraints from sedimentology and detrital zircon and rutile in the Sleat and Torridon groups, Scotland. Precambrian Res. 295, 67–89.
Li, S.X., He, B., Yang, B., Wei, Z.F., Tao, G., Gan, B.P., Zhao, F., Sun, P.Y., Zhao, Z.G., Huang, P.F., 2023. Zircon U-Pb geochronology and geochemistry of the Tagelake monzogranites in South Tianshan block: constraints on crustal magmatic origin and tectonic setting. Chin. Geol. 50 (2), 622–639 in Chinese with English abstract.
Li, S.Z., Li, X.Y., Wang, G.Z., Liu, Y.M., Wang, Z.C., Wang, T.S., Cao, X.Z., Guo, X.Y., Somerville, Ian, Li, Y., Zhou, J., Dai, L.M., Jiang, S.H., Zhao, H., Wang, Y., Wang, G., Yu, S., 2019. Global Meso-Neoproterozoic plate reconstruction and formation mechanism for Precambrian basins: constraints from three cratons in China. Earth Sci. Rev. 198 (12), 1–28.
Li, W., Yao, J.L., Zhao, G.C., Han, Y.G., Liu, Q., Zhang, D.H., 2025. Reconstructing tarim within Rodinia: constraints from early tonian accretionary and collisional records in the Altyn belt. Precambrian Res. 416, 107605.
Li, Y.J., Sun, L.D., Hu, S.L., Song, W.J., Wang, G.L., Tan, Z.J., 2003. ^{40}Ar-^{39}Ar geochronology of the granite and diorite revealed at the bottom of Tacan 1, the deepest well in China. Acta Petrol. Sin 19 (3), 530–536 in Chinese with English abstract.
Lin, W., Chu, Y., Ji, W.B., Zhang, Z.P., Shi, Y.H., Wang, Z.Y., Li, Z., Wang, Q.C., 2013. Geochronological and geochemical constraints for a middle paleozoic continental arc on the northern margin of the tarim block: implications for the paleozoic tectonic evolution of the South Chinese Tianshan. Lithosphere 5 (4), 355–381.
Long, X.P., Yuan, C., Sun, M., Zhao, G.C., Xiao, W.J., Wang, Y.J., Yang, Y.H., Hu, A.Q., 2010. Archean crustal evolution of the northern Tarim craton, NW China: zircon U-Pb and Hf isotopic constraints. Precambrian Res. 180 (3–4), 272–284.
Long, X.P., Yuan, C., Sun, M., Kroner, A., Zhao, G.C., Wilde, S., Hu, A.Q., 2011. Reworking of the Tarim Craton by underplating of mantle plume–derived magmas: evidence from Neoproterozoic granitoids in the Kuluketage area, NW China. Precambrian Res. 187 (1–2), 1–14.
Long, X.P., Sun, M., Yuan, C., Kröner, A., Hu, A.Q., 2012. Zircon REE patterns and geochemical characteristics of Paleoproterozoic anatectic granite in the northern Tarim Craton, NW China: implications for the reconstruction of the Columbia supercontinent. Precambrian Res. 222–223, 474–487.
Ning, F., Yun, J.B., Li, J.J., Song, H.M., Zhao, L.D., 2021. Structural characteristics and exploration prospects of the southwesternmargin of Bachu uplift,Tarim Basin. Oil Gas Geol. 42 (2), 299–308 in Chinese with English abstract.
Niu, Y.L., 2021. Lithosphere thickness controls the extent of mantle melting, depth of melt extraction and basalt compositions in all tectonic settings on Earth - a review and new perspectives. Earth Sci. Rev. 217, 103614.
Rainbird, R., Heaman, L.M., Young, G., 1992. Sampling Laurentia: detrital zircon geochronology offers evidence for an extensive Neoproterozoic river system originating from the Grenville orogen. Geology 20, 351–354.
Santosh, M., Sajeev, K., Li, J.H., 2006. Extreme crustal metamorphism during Columbia supercontinent assembly: evidence from northnorth China craton. Gondwana Res. 10 (3–4), 256–266.
Shu, L.S., Deng, X.L., Zhu, W.B., Ma, D.S., Xiao, W.J., 2011. Precambrian tectonic evolution of the tarim block, Nw China: new geochronological insights from the Quruqtagh Domain. J. Asian Earth Sci. 42 (5), 774–790.
Sui, Q.L., 2021. Genesis of Magmatic Rocks in Western Kunlun Orogenic Belt and Implications on the Evolution of Proto-Palaeo Tethys Ocean. University of Chinese Academy of Sciences in Chinese with English abstract.
Sun, X.H., Li, X., Lei, R.X., Yang, X.F., Chen, J.Z., Wu, C.Z., 2022. Geochronology and geochemistry of gneiss and migmatite from the Korla complex in the Quruqtagh block, NW China: implications for proterozoic crustal evolution of the northeastern tarim craton. Ore Geol. Rev. 150, 105127.
Wang, B., Shu, L.S., Faure, M., Jahn, B., Cluzel, D., Charvet, J., Chung, S.L., Meffre, S., 2011. Paleozoic tectonics of the southern Chinese Tianshan: insights from structural, chronological and geochemical studies of the Heiyingshan ophiolitic mélange (NW China). Tectonophysics 497 (1), 85–104.
Wang, C., Liu, L., He, S.P., Yang, W.Q., Cao, Y.T., Zhu, X.H., Li, R.S., 2013. Early Paleozoic magmatism in west Kunlun: constraints from geochemical and zircon U-Pb-Hf isotopic studies of the Bulong granite. Chin. J. Geol 48 (4), 997–1014 in Chinese with English abstract.
Wang, C., Liu, L., Wang, Y.H., He, S.P., Li, R.S., Li, M., Yang, W.Q., Cao, Y.T., Collins, A. S., Shi, C., Wu, Z.N., 2015. Recognition and tectonic implications of an extensive Neoproterozoic volcano-sedimentary rift basin along the southwestern margin of the Tarim Craton, northwestern China. Precambrian Res. 257, 65–82.
Wang, P., Zhao, G.C., Han, Y.G., Liu, Q., Yao, J.L., Yu, S., Li, J.H., 2020a. Timing of the final closure of the Proto-Tethys Ocean: constraints from provenance of early paleozoic sedimentary rocks in West Kunlun, NW China. Gondwana Res. 84, 151–162.
Wang, P., Zhao, G.C., Liu, Q., Han, Y.G., Yao, J.L., Li, J.H., 2020b. Zircons from the Tarim basement provide insights into its positions in Columbia and Rodinia supercontinents. Precambrian Res. 341, 105621.
Wang, Q.H., Xu, Z.P., Zhang, R.H., Yang, H.J., Yang, X.Z., 2024. New fields, new types of hydrocarbon explorations and their resource potentials in Tarim Basin. Acta Petrol. Sin. 45 (1), 15–32 in Chinese with English abstract.
Wang, X.D., Lv, X.B., Cao, X.F., Wang, Y.F., Liu, W., 2017. Palaeo-Mesoproterozoic magmatic and metamorphic events from the Kuluketage block, northeast Tarim Craton: geochronology, geochemistry and implications for evolution of Columbia. Geol. J. 55, 1.
Wang, X.S., Klemd, R., Gao, J., Jiang, T., Li, J.L., Xue, S.C., 2018. Final assembly of the Southwestern central Asian orogenic belt as constrained by the evolution of the South Tianshan orogen: links with Gondwana and Pangea. J. Geophys. Res. Solid Earth 123 (9), 7361–7388.
Wang, Y.X., Wang, J.R., Zhou, X.L., Wang, H.T., Di, P.F., Wang, X.W., Chen, W.F., 2017. The cracking of Columbia supercontinent: evidence from the Dahongshan A-type granite in the southeastern tarim craton. Acta Geol. Sin. 91 (11), 2369–2386 in Chinese with English abstract.
Wei, G.Q., Jia, C.Z., Li, B.L., Chen, H.L., 2002. The southern margin of Tarim Basin is Siluran-Devonian foreland basin. Chin. Sci. Bull. 47 (S1), 44–48 in Chinese.
Wei, X.P., 2018. Spatial-temporal Pattern, Petrogenesis and Tectonic Implications of the Triassic Granitoids from the Western Kunlun Orogen, Northwestern China. University of Chinese Academy of Sciences in Chinese with English abstract.
Wen, B., Evans, D.A.D., Wang, C., Li, Y.X., Jing, X.Q., 2018. A positive test for the Greater Tarim Block at the heart of Rodinia: mega-dextral suturing of supercontinent assembly. Geology 46 (8), 687–690.
Wu, C.L., Yao, S.Z., Zeng, L.S., Yang, J.S., Wooden, J., Chen, S.Y., Mazadab, F., 2007. Characteristics and zircon SHRIMP U-Pb dating of the Bashkautic-Smirburak granite complex in northern Altun. Sci. China Earth Sci. 37 (1), 10–26 in Chinese.
Wu, Y.Q., Jiang, F.J., Xu, Y.L., Guo, J., Xu, T.W., Hu, T., Shen, W.B., Zheng, X.W., Chen, D., Jiang, Q., Yu, S.X.Y., 2025. Middle Eocene Climatic Optimum drove palaeoenvironmental fluctuations and organic matter enrichment in lacustrine facies of the Bohai Bay Basin, China. Palaeogeogr. Palaeoclimatol. Palaeoecol. 659, 112665.
Wu, C.L., Lei, M., Wu, D., Zhang, X., Chen, H.J., Li, T.X., 2016. Zircon U-Pb dating of paleozoic granites from south Altun and response of the magmatic activity to the tectonic evolution of the Altun orogenic belt. Acta Geol. Sin. 90 (9), 2276–2315 in Chinese with English abstract.
Wu, G.H., Zhang, C.Z., Wang, H., Liu, Y.K., Li, J.J., 2009. Zircon SHRIMP U-Pb age of granodiorite of the Tacan 1 well in the central Tarim basin, China. Geol. Bull. China, 2009 28 (5), 568–571 in Chinese with English abstract.
Wu, G.H., Sun, J.H., Guo, Q.Y., Tang, T., Chen, Z.Y., Feng, X.J., 2010. The distribution of detrital zircon U-Pb ages and its significance to precambrian basement in Tarim Basin. Acta Geosci. Sin. 31 (1), 65–72 in Chinese with English abstract.
Wu, G.H., Xiao, Y., Bonin, B., Ma, D.B., Li, X., Zhu, G.Y., 2018. Ca. 850 Ma magmatic events in the Tarim Craton: age, geochemistry and implications for assembly of Rodinia supercontinent. Precambrian Res. 305, 489–503.
Wu, G.H., Yang, S., Meert, J.G., Xiao, Y., Chen, Y.Q., Wang, Z.C., Li, X., 2020. Two phases of paleoproterozoic orogenesis in the tarim craton: implications for Columbia assembly. Gondwana Res. 83, 201–216.
Wu, H.X., Zhang, F.Q., Dilek, Y., Chen, H.L., Wang, C.Y., Lin, X.B., Cheng, X.G., Zhu, K. Y., 2022. Mid-neoproterozoic collision of the tarim craton with the yili-central tianshan block towards the final assembly of supercontinent Rodinia: a new model. Earth Sci. Rev. 228, 103989.
Xin, H.T., Zhao, F.Q., Luo, Z.H., Liu, Y.S., Wan, Y.S., Wang, S.Q., 2011. Determination of the paleoproterozoic geochronological framework in Aqtashtagh area in southeastern tarim,China,and its geological significance. Acta Geol. Sin. 85 (12), 1977–1993 in Chinese with English abstract.
Xu, B., Jian, P., Zheng, H.F., Zou, H.B., Zhang, L.F., Liu, D.Y., 2005. U-Pb zircon geochronology and geochemistry of Neoproterozoic volcanic rocks in the Tarim Block of northwest China: implications for the breakup of Rodinia supercontinent and Neoproterozoic glaciations. Precambrian Res. 136 (2), 107–123.
Xu, B., Xiao, S.H., Zou, H.B., Chen, Y., Li, Z.X., Song, B., Liu, D.Y., Zhou, C.M., Yuan, X.L., 2009. SHRIMP zircon U-Pb age constraints on Neoproterozoic Quruqtagh diamictites in NW China. Precambrian Res. 168 (3–4), 247–258.
Xu, B., Zou, H.B., Chen, Y., He, J.Y., Wang, Y., 2013. The Sugetbrak basalts from northwestern tarim block of northwest China: geochronology, geochemistry and implications for Rodinia breakup and ice age in the late neoprotero-zoic. Precambrian Res. 236, 214–226.
Xu, Z.Q., Li, S.T., Zhang, J.X., Yang, J.S., He, B.Z., Li, H.B., Lin, C.S., Cai, Z.H., 2011. Paleo-Asian and Tethyan tectonic systems with docking the Tarim block. Acta Petrol. Sin. 27 (1), 1–22 in Chinese with English abstract.
Xu, Z.Q., He, B.Z., Zhang, C.L., Zhang, J.X., Wang, Z.M., Cai, Z.H., 2013. Tectonic framework and crustal evolution of the Precambrian basement of the Tarim Block in NW China: new geochronological evidence from deep drilling samples. Precambrian Res. 235, 150–162.

Yang, H.J., Wu, G.H., Kusky, T.M., Chen, Y., Xiao, Y., 2018. Paleoproterozoic assembly of the north and south Tarim terranes: new insights from deep seismic profiles and Precambrian granite cores. Precambrian Res. 305 (2), 151–165.
Yang, X., Xu, X.H., Qian, Y.X., Chen, Q.L., Chu, C.L., Jiang, H.J., 2014. Discussion on regional differences of basement composition of the Tarim Basin, NW China. Geotect. Metallogenia 38 (3), 544–556 in Chinese with English abstract.
Yuan, C., Sun, M., Zhou, M.F., Zhou, H., Xiao, W.J., Li, J.L., 2002. Tectonic evolution of the West Kunlun: geochronologic and geochemical constraints from Kudi granitoids. Int. Geol. Rev. 44, 653–669.
Zhang, B., Chen, W., Yu, S., Yin, J.Y., Li, J., Sun, J.B., Yang, L., Yang, J., 2014. Subduction process of South Tianshan ocean during paleozoic. Acta Petrol. Sin. 30 (8), 2351–2362 in Chinese with English abstract.
Zhang, C.L., Dong, Y.G., Zhao, Y., Wang, A.G., Guo, K.Y., 2003a. Geochemistry of mesoproterozoic volcanic rocks in the western Kunlun mountains:evidence for plate tectonic evolution. Acta Geol. Sin. Engl. Ed 77 (2), 237–245.
Zhang, C.L., Shen, J.L., Wang, A.G., Zhao, Y., Guo, K.Y., Li, C.H., 2003b. Caledonian low-temperature granulite-facies metamorphism in the West Kunlun orogenic belt - SHRIMP chronological evidence from zircon. Chin. J. Geochem. 22 (4).
Zhang, C.L., Li, Z.X., Li, X.H., Ye, H.M., Wang, A.G., Guo, K.Y., 2006. Neoproterozoic bimodal intrusive complex in the southwestern tarim block, northwest China: age, geochemistry, and implications for the rifting of Rodinia. Int. Geol. Rev. 48 (2), 112–128.
Zhang, C.L., Li, Z.X., Li, X.H., Ye, H.M., 2007. Early Palaeoproterozoic high-K intrusive complex in southwestern Tarim Block, NW China: age, geochemistry and implications for the Paleoproterozoic tectonic evolution of Tarim. Gondwana Res. 12, 101–112.
Zhang, C.L., Li, Z.X., Li, X.H., Ye, H.M., 2009. Neoproterozoic mafic dyke swarms in the northern margin of the Tarim Block, NW China: age, geochemistry, petrogenesis and tectonic implications. J. Asian Earth Sci. 35 (2), 167–179.
Zhang, C.L., Yang, D.S., Wang, H.Y., Takahashi, Y., Ye, H.M., 2011. Neoproterozoic mafic–ultramafic layered intrusion in Quruqtagh of northeastern Tarim Block, NW China: two phases of mafic igneous activity with different mantle sources. Gondwana Res. 19 (1), 177–190, 2011.
Zhang, C.L., Li, H.K., Santosh, M., Li, Z.X., Zou, H.B., Wang, H.Y., Ye, H.M., 2012. Precambrian evolution and cratonization of the tarim block, NW China: petrology, geochemistry, Nd-isotopes and U-Pb zircon geochronology from archaean gabbro-TTG-potassic granite suite and paleoproterozoic metamorphic belt. J. Asian Earth Sci. 47, 5–20.
Zhang, C.L., Zou, H.B., Li, H.K., Wang, H.Y., 2013. Tectonic framework and evolution of the tarim block in NW China. Gondwana Res. 23 (4), 1306–1315.
Zhang, C.L., Ye, X.T., Zou, H.B., Chen, X.Y., 2016. Neoproterozoic sedimentary basin evolution in southwestern Tarim, NW China: new evidence from field observations, detrital zircon U-Pb ages and Hf isotope compositions. Precambrian Res. 280, 31–45.
Zhang, C.L., Zou, H.B., Ye, X.T., Chen, X.Y., 2018. Timing of subduction initiation in the Proto-Tethys Ocean: evidence from the cambrian gabbros from the NE Pamir Plateau. Lithos 314, 40–51.
Zhang, C.L., Zou, H.B., Ye, X.T., Chen, X.Y., 2019. Tectonic evolution of the West Kunlun orogenic belt along the northern margin of the Tibetan plateau: implications forthe assembly of the tarim terrane to Gondwana. Geosci. Front. 10 (3), 973–988.
Zhang, H.S., Ji, W.H., Ma, Z.P., Gao, X.F., Sun, C., Hong, J., Lv, P.R., 2020. Geochronology and geochemical study of theCambrian andesite in tianshuihai terane: implications for the evolution of the Proto-Tethys Ocean in the West Kunlun-Karakoram orogenic belt. Acta Petrol. Sin. 36 (1), 257–278 in Chinese with English abstract.
Zhang, J., Li, H.K., Zhang, C.L., Tian, H., Zhong, Y., Ye, X.T., 2018. New evidence forthe breakup of the Columbia supercontinent from the northeastern margin of Tarim Craton: rock geochemistry, zircon U-Pb geochronology and Hf-O isotopiccompositions of the ca.1.55 Ga diabase sills in the Kuruktag area. Earth Sci. Front. 25 (6), 106–123 in Chinese with English abstract.
Zhang, Z.Y., Zhu, G.Y., Chen, W.Y., Wu, L., Ren, R., Zhang, C.L., 2024. Cryogenian-Cambrian tectono-sedimentary evolution, paleoclimate and environment effects, and formation of petroleum resources in the Tarim Block. Earth Sci. Rev. 248, 104632.
Zhao, G.C., Cawood, P.A., Wilde, S.A., Sun, M., 2002. Review of global 2.1–1.8 Ga orogens: implications for a pre-Rodinia supercontinent. Earth Sci. Rev. 59 (1–4), 125–162.
Zhao, P., He, J.Y., Deng, C.L., Chen, Y., Mitchell, R.N., 2021. Early neoproterozoic (870-820 Ma) amalgamation of the tarim craton (northwestern China) and the final assembly of Rodinia. Geology 49 (11), 1277–1282.
Zhao, Z.Y., Zhang, Z.C., Santosh, M., Huang, H., Cheng, Z.G., Ye, J.C., 2015. Early paleozoic magmatic record from the northern margin of the tarim craton: further insights on the evolution of the central Asian orogenic belt. Gondwana Res. 28 (1), 328–347.
Zhou, T., Ge, R.F., Zhu, W.B., Wu, H.L., 2021. Is there a grenvillian orogen in the southwestern tarim craton? Precambrian Res. 354, 106053.
Zhu, W.B., Zhang, Z.Y., Shu, L.S., Lu, H.F., Su, J.B., Yang, W., 2008. SHRIMP U–Pb zircon geochronology of Neoproterozoic Koral mafic dykes in the northern Tarim Block, NW China: implications for the long–lasting breakup process of Rodinia. J. Geol. Soc. London 165, 887–890.
Zong, K.Q., Liu, Y.S., Zhang, Z.M., He, Z.Y., Hu, Z.C., Guo, J.L., Kang, C., 2013. The generation and evolution of Archean continental crust in the Dunhuang block, northeastern Tarim craton, northwestern China. Precambrian Res. 235 (34), 251–263.